Invited paper

Photorefractive waveguides in oxide crystals: fabrication, properties, and applications

D. Kip

Universität Osnabrück, Fachbereich Physik, D-49069 Osnabrück, Germany
(Fax: +49-541/969-2670, E-mail: dkip@physik.uni-osnabrueck.de)

Abstract. In several oxide crystals the refractive index can be changed by inhomogeneous illumination, and these photorefractive properties have allowed for a wide variety of applications in optical data storage and dynamic holography. The high light intensities that are inherent in waveguide geometries make it relatively easy to observe photorefractive effects in waveguide structures, too. On the one hand, these effects are feared as optical damage, as they can degrade the performance of integrated optical devices. On the other hand, optical wave mixing in photorefractive waveguides is of considerable interest for the development of nonlinear optical components. A review of the results of recent research on the fabrication, investigation, and applications of photorefractive waveguides is given. The formation and photorefractive properties of $LiNbO_3$, $LiTaO_3$, $BaTiO_3$, $KNbO_3$, $Sr_xBa_{1-x}Nb_2O_6$ ($0.25 \leq x \leq 0.75$, SBN), and $Bi_{12}(Si, Ti, Ge)O_{20}$ (BSO, BTO, BGO) waveguides are discussed. Furthermore, the suitability of photorefractive waveguides for nonlinear optical components is demonstrated in some examples.

PACS: 42.65; 42.82; 78.20

Photorefractive effects in optical waveguides link two interesting research areas: light-induced refractive index changes in optical materials, and waveguide structures that are the basis for integrated optical devices.

Since the discovery by Ashkin et al. [1] more than three decades ago, light-induced refractive index changes in oxide crystals have attracted great attention because of their potential use in holographic storage and optical communications [2, 3]. These photorefractive effects can be explained by the optical excitation of charge carriers (electrons and/or holes) that migrate in the crystal and are subsequently trapped at new sites. Thus a space charge field builds up that modulates the refractive index of the material via the electro-optic effect.

In integrated optics, several optical components, such as channel waveguides, power dividers, or modulators, are integrated on a suitable substrate material [4, 5]. The performance of such devices is considerably reduced if device properties depend on light intensity because of undesired photorefractive effects. On the other hand, photorefractive effects in waveguides are of considerable interest for efficient wave mixing of optical beams. Because of the high light intensities that can be easily obtained in waveguides, the typical buildup time of refractive index gratings can be decreased by orders of magnitude when compared to bulk samples.

Photorefractive effects in waveguides were outlined in an earlier review by Wood, Cressman, Holman, and Verber [6], giving an excellent summary of the work that had been done until 1986. However, as this is quite an active area of research, many new and interesting results have been published in the last years. In this article more recent results of research work on the formation, investigation methods, properties, and applications of photorefractive waveguides are reviewed. In order not to repeat parts of the review cited above, in some passages references that provide a more current overview of the respective topic are given.

In the first section, different methods of both waveguide fabrication and additional surface doping of the substrates are discussed, and a brief summary of thin film deposition techniques is given that may be of interest for future waveguide devices. The second section describes experimental methods for the reconstruction of refractive index profiles and the measurement of electro-optical properties of single-crystalline layers, as well as different holographic techniques that have been used for the investigation of photorefractive waveguides. The main part of this work (Sect. 3) consists of a detailed discussion of the photorefractive properties of $LiNbO_3$, $LiTaO_3$, $BaTiO_3$, $KNbO_3$, $Sr_xBa_{1-x}Nb_2O_6$ ($0.25 \leq x \leq 0.75$, SBN), and $Bi_{12}(Si, Ti, Ge)O_{20}$ (BSO, BTO, BGO) planar and channel waveguides as well as single-crystalline fiber-like crystals. Where it is possible, photorefractive effects in samples fabricated by different techniques are compared

with each other. In a final part, the suitability of waveguides with optimized photorefractive properties for nonlinear optical components is demonstrated in some examples, including narrow-band holographic filters, optical phase conjugation, and all-optical switching and routing.

1 Waveguide fabrication

This section describes the different methods that can be used for the fabrication of waveguides in photorefractive crystals. Diffusion, ion exchange, implantation of ions, deposition of epitaxial thin layers, and alternative techniques are discussed.

1.1 Diffusion

Many metal ions can be diffused into $LiNbO_3$ and $LiTaO_3$ to form low-loss waveguiding layers or channels, whereas the same technique has failed so far for most other ferroelectric crystals such as $BaTiO_3$, $KNbO_3$, or SBN. Titanium diffusion into $LiNbO_3$ is by far the most common technique for waveguide fabrication. On the other hand, diffusion is also an easy method of increasing the photorefractive sensitivity by surface doping of the waveguide substrates.

1.1.1 Titanium diffusion. The diffusion of thin films of titanium evaporated or sputtered onto the substrate surface [7] is a widely used method for waveguide formation in $LiNbO_3$ and in part also in $LiTaO_3$ crystals, and most of the integrated optical devices available today are based on titanium-diffused $LiNbO_3$ waveguides. The diffusion process itself consists of several complex steps [8, 9] and is still not fully understood. A highly simplified description of titanium diffusion into $LiNbO_3$ reads as follows. At a temperature of about 500 °C, titanium is oxidized to TiO_2, and above 600 °C $LiNb_3O_8$ epitaxial crystallites are formed at the surface, connected with a loss of lithium. For temperatures larger than 950 °C a $(Ti_{0.65}Nb_{0.35})O_2$ mixed oxide appears, which acts as the diffusion source for titanium indiffusion. With increasing annealing time titanium diffuses deeper into the crystal, and the titanium–niobium oxide layer decomposes.

In $LiNbO_3$ the extraordinary refractive index increases linearly with titanium concentration, whereas the ordinary index shows a slightly nonlinear behavior [10]. Larger changes are obtained for extraordinarily polarized light. No significant reduction of the electro-optic or nonlinear optical coefficients has been reported.

Diffusion of titanium has been used to produce waveguides in $LiTaO_3$ [11], too. The low diffusion coefficient requires temperatures above 1000 °C, which is much higher than the Curie temperature of about 620 °C. Thus the samples have to be polarized again after diffusion to avoid degradation of the electro-optic properties.

1.1.2 Iron and copper diffusion. The photorefractive sensitivity of waveguides in ferroelectric crystals can be strongly enhanced by surface doping of the substrate. The commonly used method is that of indiffusion of suitable metal ions, for example, iron or copper. This technique has been combined with titanium diffusion into $LiNbO_3$ and $LiTaO_3$ substrates [12, 13]. The fabricated $LiNbO_3$:Ti:Fe, Cu and
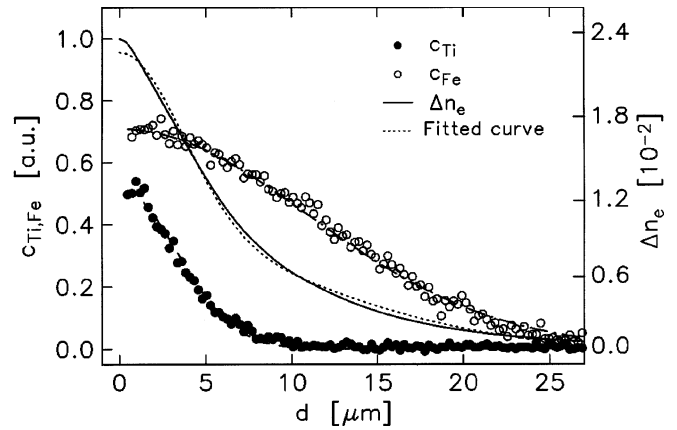
Fig. 1. Concentration profiles c_{Ti}, c_{Fe}, and reconstructed extraordinary refractive index profile Δn_e of a planar $LiNbO_3$:Ti:Fe waveguide [13]. The dopant profiles c_{Ti}, c_{Fe}, can be described by Gaussian functions (*dashed lines*, partly concealed). The reconstructed refractive index profile can be approximated by a linear superposition of iron and titanium concentration profiles (*dotted line*)

$LiTaO_3$:Ti:Fe waveguides have considerably improved photorefractive properties, with sensitivities that are orders of magnitude higher than those of undoped substrates.

For the fabrication of waveguides with tailored properties, detailed knowledge of the index change as a function of dopant concentration is necessary. We have shown that both refractive indices of $LiNbO_3$ increase nearly linearly with iron concentration [13], whereas index changes by copper are small and negative [14]. Waveguides can be fabricated by indiffusion of iron alone [15, 16]. Furthermore, dark conductivity is distinctly enhanced by iron indiffusion and may exceed photoconductivity for strong doping [17]. As an example, in Fig. 1 our results on the concentration profiles of the indiffused titanium and iron in a planar $LiNbO_3$:Ti:Fe waveguide are given [13]. The impurity concentrations have been measured with the focused electron beam of a microprobe, which scans the polished endface of the sample. The reconstructed refractive index profile Δn_e can be approximated fairly well by the superposition of the two Gaussian distributions of titanium and iron concentration.

1.1.3 Other diffusion sources. A large number of other metals can be diffused into $LiNbO_3$ to form waveguiding layers, for example, vanadium, nickel, niobium, cobalt, silver, or gold [7], but the best results have been obtained by using titanium. The diffusion of zinc into $LiNbO_3$ has been found to produce low-loss waveguides with high resistance to photorefractive damage [18]. Both refractive indices are increased, whereas the diffusion constant for zinc into $LiNbO_3$ is two orders of magnitude higher than for titanium. For $LiTaO_3$ crystals niobium is an alternative diffusion source to titanium that produces low-loss waveguides, too [19].

Heating of single-crystalline $LiNbO_3$ or $LiTaO_3$ to temperatures above 600 °C leads to a loss of Li or Li_2O at the crystal surface. Lithium out-diffusion has been found to increase the extraordinary refractive index over the whole crystal surface, while the ordinary refractive index is reduced [20]. A waveguiding layer is formed for extraordinarily polarized light, and the possibility of low-loss single as well as multimode waveguide fabrication was recognized

early [21]. For the fabrication of channel waveguides by titanium diffusion this is an undesired effect, as it reduces the optical confinement in the indiffused stripes. Consequently, different possibilities have been described to prevent lithium out-diffusion during annealing [22, 23], and today titanium diffusion in a water-vapor or lithium-rich atmosphere are common techniques for channel waveguide formation.

1.2 Ion exchange

To raise the refractive index of a medium the molecular structure of the material has to be altered. For some substrate crystals, this can be done by the simple and cheap method of ion exchange. Here the proton exchange technique in $LiNbO_3$ and $LiTaO_3$ has proved to result in good quality waveguides, which are in particular well suited for applications where high intensities occur, for example, second-harmonic generation or waveguide lasers. Different sources for the ion exchange may be used, and proton exchange can be combined with surface doping of the waveguiding layer.

1.2.1 Proton exchange (PE). This is a low-temperature process ($T < 250\,°C$) which has been used successfully for waveguide fabrication in $LiNbO_3$ and $LiTaO_3$ [24, 25]. Basically, hydrogen that is provided by an appropriate acid is exchanged for lithium ions of the crystal. Only partial exchange is necessary for the formation of waveguides, and the chemical reaction, in this case for $LiNbO_3$, can be written as

$$LiNbO_3 + xH^+ \rightarrow Li_{1-x}H_xNbO_3 + xLi^+. \tag{1}$$

Here the value of x, $0 \leq x \leq 1$, is the exchange degree. The most widely used technique is the immersion of the substrate in a bath of molten benzoic acid. To reduce the acidity of the melt it can be diluted by the addition of some mol percent of lithium benzoate [24]. Other methods exist, using alternative hydrogen sources such as phosphoric acid [26, 27], or sulfuric acid [28]. Recent reviews of the proton exchange technique can be found in [29, 30].

Proton exchange increases the extraordinary refractive index, while the ordinary index is reduced [24]. Without further treatment, the obtained refractive index profiles are nearly step-like. The size of the maximum index change depends on the used acid. Typical values for benzoic acid are $\delta n_e = 0.12$, $\delta n_o = -0.05$ for $LiNbO_3$ [24], and $\delta n_e = 0.02$, $\delta n_o \approx 0$ for $LiTaO_3$ [31, 32]. The largest changes of the extraordinary refractive index of $\delta n_e = 0.145$ [26] for $LiNbO_3$ have been obtained by using phosphoric acid. However, even when the ordinary refractive index is decreased at the substrate surface, weak waveguiding for ordinarily polarized modes has been observed [33, 34]. This may be due to the formation of a thin layer of a rhombohedral β_1-phase of $Li_{1-x}H_xNbO_3$ [35] directly at the proton diffusion front, with a lower refractive index than the upper proton-exchanged layer, i.e., ordinarily polarized light is (weakly) guided by reflection at the created optical barrier.

$LiNbO_3$ channel waveguides fabricated with pure benzoic acid have typical propagation losses between 0.5 and $1\,cm^{-1}$ for extraordinarily polarized light, whereas lower values of about $0.2\,cm^{-1}$ have been reported for the use of phosphoric acid [26]. A significant degradation of electro-optic and non-linear optical properties of proton-exchanged $LiNbO_3$ waveguides was found very early [36] and can be explained by the lattice disorder and mixture of different phases, especially in strongly exchanged layers [35, 37]. Only slightly reduced electro-optic coefficients have been obtained for waveguides exchanged in lithium benzoate buffered acids or for samples annealed after the exchange [38, 39], and a full recovery of the electro-optic performance has been achieved by post-exchange annealing treatment at high temperatures ($T \approx 350\,°C$) [40]. These so-called annealed proton-exchanged (APE) waveguides have a graded refractive index profile. The waveguiding layer is completely converted to the α-phase of $Li_{1-x}H_xNbO_3$ [35], with an exchange degree of $x < 0.12$, corresponding to an extraordinary refractive index change of $\delta n_e < 0.025$ [34]. Furthermore, for APE waveguides very small loss coefficients of about $0.03\,cm^{-1}$ have been measured [41].

1.2.2 Combined proton and copper exchange. Waveguides in $LiNbO_3$ and $LiTaO_3$ with strongly enhanced photorefractive sensitivity can be fabricated by proton exchange combined with a successive copper exchange from melts containing Cu^+ or Cu^{2+} ions [34, 42]. As this technique of copper doping is a low-temperature process well below the Curie temperature of $LiTaO_3$, it is of particular interest for the fabrication of photorefractive waveguides in this material.

In a first step, proton-exchanged waveguides are formed by normal treatment of the substrate in molten benzoic acid. In a second step, protons of the $Li_{1-x}H_xNbO_3$ or $Li_{1-x}H_xTaO_3$ layers, respectively, are exchanged for either Cu^+ or Cu^{2+} ions. The melts for copper exchange consist of benzoic acid and some mol percent of copper acetate [42, 43] or copper oxide [34]. Final annealing treatment for several hours at temperatures of 350 to $400\,°C$ has been found to be necessary to reduce absorption loss, to recover electro-optic coefficients, and to increase both steady-state diffraction efficiency and holographic sensitivity in the samples.

For $LiNbO_3$ waveguides fabricated by combined proton and copper exchange we have measured light-induced refractive index changes up to 3×10^{-3} [34], an increase of two orders of magnitude compared to samples fabricated by proton exchange alone. For $LiTaO_3$ waveguides we have obtained similar values [42], too.
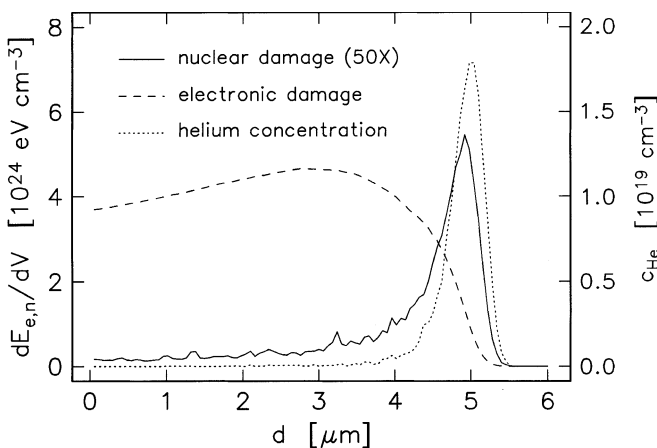
1.2.3 Metal ion exchange. The ion exchange using potassium and sodium salts is commonly used for the fabrication of waveguide structures on glass substrates. The same technique has been applied to the formation of waveguiding layers in $LiNbO_3$ [33] and $LiTaO_3$ [44] crystals, too. Ion exchange in a mixture of potassium nitrate and silver nitrate has been shown to increase both the ordinary and the extraordinary refractive index in $LiNbO_3$ [45]. For $LiTaO_3$ both waveguide formation and additional surface doping have been achieved by ion exchange in an eutectic composition of potassium chloride and copper chloride, or by using a mixture of zinc, potassium, sodium, and copper sulfate [44].

1.3 Ion implantation

The implantation of light ions such as H^+ and He^+ with an energy of some MeV has been successfully used for waveguide formation in a wide range of optical materials, including photorefractive ferroelectrics and sillenites. The first ion-implanted waveguide structure was fabricated in LiNbO$_3$ [46], but the method of ion implantation is especially well suited for perovskites such as BaTiO$_3$ and KNbO$_3$ [47–49] and the crystals of the tungsten–bronze family, in particular SBN [51], where low-temperature phase transitions and large chemical inertness make other waveguide formation techniques more difficult.

A computer modelling of the implantation can be made by a TRIM simulation [52] that uses a Monte-Carlo method. Our results of such a simulation of He^+ implantation into lead germanate is shown in Fig. 2 [50]. During their path into the crystal, the implanted ions slow down because of energy loss from interactions with electrons and nuclei of the crystal. At higher energy of the incoming ions, electronic excitation of the crystal ions is the dominant loss mechanism. Depending on the substrate material, color and scattering centers may be created, and in some cases post-annealing of the sample has been used to reduce optical losses [53]. In a low energy range of some keV, nuclear collision is the most important mechanism for energy transfer between the implanted ion and the crystal ions. In principle, this damage can lead to an amorphization of the former ordered structure, and the resulting expansion of the atomic packaging causes a reduction of the refractive index of the material. As can be seen in Fig. 2, the nuclear damage per crystal volume has a sharp maximum at a depth of about 5 μm below the substrate surface. Consequently, a well-defined buried, damaged layer with a reduced refractive index is formed, and light can be guided by total internal reflection at this barrier.

The loss mechanism in ion-implanted waveguides is rather complex and consists of different parts, namely material and implantation-induced absorption, surface scattering, and tunneling losses. A detailed theoretical and experimental

investigation of mode propagation loss for KNbO$_3$ waveguides can be found in [54].

The ion-dose dependence of the refractive-index decrease generally shows a saturation behavior, whereas the initial growth rate and the saturation level depend on ion energy [55]. A typical size of the refractive-index decrease is about 5% of the substrate value; deeper barriers up to 10% have been obtained for KNbO$_3$ [56].

Because of the well-defined penetration depth of the ions, the refractive index profiles obtained by ion implantation are nearly step-like, particularly for higher ion energies, when the ions are implanted deep in the substrate. For lower energies and corresponding smaller penetration depths of the ions of only a few μm, for example, single-mode waveguides, deviations from the step-like form may occur because of the nuclear recoil energy growing with increasing depth, which leads to damage even in the near-surface region.

For a low dose of the implanted ions in the range of some 10^{13} to 10^{15} cm^{-2}, a slight increase of the extraordinary refractive index has been observed for several ferroelectric crystals [57]. This effect has been used to fabricate non-leaky waveguides [58], where light is confined without the possibility of barrier tunneling. Higher doses of 10^{16} cm^{-2} and more have resulted in a decrease of both refractive indices. Furthermore, the implantation through an appropriate mask on the substrate surface has enabled the fabrication of both, single and multimode channel waveguides in various materials [57, 59].

1.4 Thin film deposition

The deposition technology of thin epitaxial layers [60, 61] has advanced dramatically during the last decades, mainly stimulated by the rapidly growing progress in microelectronics. Dozens of different deposition techniques have been developed, each of them having particular advantages for specific material compounds or applications.

The fabrication of photorefractive waveguides on the surface of a single-crystal substrate is a very cost-intensive procedure. The aim of this paragraph is to give a short overview of alternative techniques, i.e., thin film deposition, which have been recently used for the formation of single-crystalline oxide layers and which are promising for the development of nonlinear optical waveguides. Thin ferroelectric films on semiconductor substrates are also of great importance for future hybrid devices that make use of both the electronic properties of the substrate and the nonlinear optical properties of the deposited film.

1.4.1 Sputtering. A wide range of different sputtering techniques have been developed in the past, including diode, reactive, ion beam, magnetron, or bias sputtering, and nearly all oxide crystals that are of interest for waveguide applications have been fabricated in thin film form by sputtering of a suitable target material. However, control of stoichiometry and microstructure are difficult; thus only in a few cases single-crystal layers have been obtained.

A relatively new sputter method is pulsed laser deposition (PLD). In most cases light of an excimer laser is used to evaporate the target atoms, and good results have been obtained by in situ annealing of the growing film. Epitaxial films

Fig. 2. TRIM simulation of implantation of 2-MeV He$^+$ at a dose of 10^{15} cm^{-2} into lead germanate (Pb$_5$Ge$_3$O$_{11}$). Nuclear and electronic damage, i.e., energy deposition d$E_{n,e}$ by collisions of the implanted ions with nuclei and electrons, respectively, per crystal volume dV, and helium concentration c_{He}, are measured from the substrate surface

with promising nonlinear optical properties that are similar to the bulk material have been realized for LiNbO$_3$ [62], BaTiO$_3$ [63], KNbO$_3$ [64], and SBN [65].

1.4.2 Molecular beam epitaxy (MBE). This is a sophisticated, finely controlled method for growing single-crystal epitaxial films under high-vacuum conditions. Thin films are formed on the heated substrate surface by slowly evaporating the elemental or molecular constituents utilizing relatively small collimated beams. Advantages are the uniquely high precision of the layer by layer growth and the low temperature requirement for epitaxy. On the other hand, the limited growth speed for a larger film thickness of some hundred nm and the complex equipment are major limitations of this promising technique. However, several thin film ferroelectrics have been fabricated using MBE, for example, LiTaO$_3$ [66] and BaTiO$_3$ [67].

1.4.3 Liquid phase epitaxy (LPE). LPE is used for the thermally-controlled overgrowth of single-crystal films from the melt on a single-crystalline substrate. When compared to MBE, the uniformity and surface morphology are poor; but deposition rates are high. However, sometimes it is difficult to fabricate layers thinner than a few μm. The technology is relatively simple and cheap. Examples of thin ferroelectric film compounds are LiNbO$_3$ on LiTaO$_3$ substrates [68], and SBN layers on MgO [69].

1.4.4 Metal organic chemical vapor deposition. Single-crystal layers grown by the copyrolysis of various combinations of organometallic compounds and hydrides, the metal organic chemical vapor deposition (MOCVD), have achieved a great technological importance in the fabrication of fast optoelectronic devices. MOCVD offers a competitive alternative to MBE for epitaxial film fabrication. Growth rates and thickness control are satisfactory, and highly uniform layers with good surface morphology can be grown over large areas. Motivated by excellent results obtained for semiconductor devices, the fabrication of numerous ferroelectric films for application in nonlinear optics has been demonstrated [70–72].

1.5 Other fabrication techniques

Only a few alternative methods for the fabrication of photorefractive waveguides have been published in the past. Different ferroelectric layers fabricated by the sol-gel process have been obtained including BaTiO$_3$ [73] and SBN [74], but shrinking of the films during the drying resulted in small grain sizes of some tens of nm.

Channel waveguides were formed because of induced strain on the surface of a single-crystal substrate [75]. Strain is produced by a thick film deposited on the substrate surface at a temperature of a few hundred degrees Centigrade. After the sample has cooled down, different thermal expansion leads to strain on the sample surface. Small stripes are etched in the deposited layer, and waveguides are formed in the strain-free channels because of a refractive-index increase that is due to the strain-optic effect.

Another straightforward method consists in the formation of a thin coating layer with a high refractive index, for example, titanium dioxide (TiO$_2$), on a substrate material with a lower refractive index. A waveguide with a large evanescent electric field may be formed, which makes use of the nonlinear optical properties of the substrate.

2 Investigation techniques

In the following paragraphs different techniques for the reconstruction of refractive index profiles and the measurement of electro-optic coefficients, as well as holographic investigation methods that can be used for the determination of photorefractive properties are presented.

2.1 Refractive index profiles

Refractive index profiles with typical dimensions of a few μm can hardly be determined by direct measurement, in particular for waveguides in oxide crystals with relatively high refractive indices. Several reconstruction techniques have been developed that make use of a set of measured effective refractive indices $n_{\mathrm{eff},i}$ of the waveguide. For planar structures the prism coupling method (dark line spectroscopy) [76] is particularly simple and yields a resolution of better than 10^{-4} for n_{eff}.

To reconstruct the refractive index profile, two different strategies have been established. The first is to assume a family of plausible profiles that are characterized by a set of parameters. The parameters are varied until the effective refractive indices of the computed profile match the measured ones best. Good results have been obtained for ion-implanted waveguides [55, 56], where the profile form can be well predicted by using TRIM simulations. A second procedure commonly used for profile reconstruction is the inverse WKB method. Several algorithms have been published [77–79], and the results for waveguides with higher mode numbers ($i > 4$) are very satisfactory.

For channel waveguides, different numerical approximations are used to calculate the effective refractive indices of the modes of an assumed or given refractive index profile, for example, the methods of finite differences or finite elements. The form of the refractive index profile is varied until the calculated mode profiles fit the measured light distribution of the excited waveguide modes.

2.2 Electro-optic properties

The electro-optic properties of a waveguide structure may be changed because of the fabrication process when compared to the bulk material. Thus several techniques have been used to determine electro-optic coefficients in both planar and channel waveguides.

The measurement of electro-optic coefficients in planar waveguides has been carried out by using attenuated total reflection (ATR) spectroscopy, a method that is well known from the investigation of electro-optic polymer layers [80].

Depth profiling of electro-optic coefficients in graded index waveguides becomes possible by excitation of different modes of the sample. An example is given in Fig. 3 where we
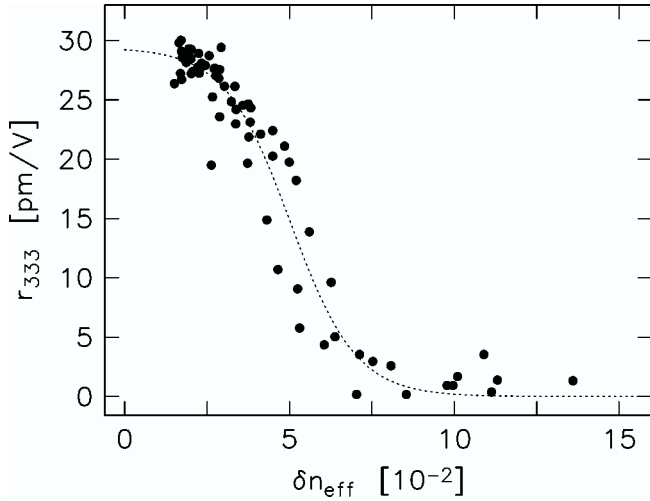
Fig. 3. Electro-optic coefficient r_{333} as a function of the difference $\delta n_{\mathrm{eff}} = n_{\mathrm{eff}} - n_{\mathrm{e}}$ of effective extraordinary refractive index and the substrate index for a proton-exchanged LiNbO$_3$ waveguide [34]. The *dotted line* is merely a guide for the eye

have measured the coefficient r_{333} of a PE LiNbO$_3$ waveguide as a function of the difference $\delta n_{\mathrm{eff}} = n_{\mathrm{eff}} - n_{\mathrm{e}}$ [34]. Here n_{eff} is the effective extraordinary refractive index of the mode, and n_{e} is the substrate index. Between separate measurements, the sample was annealed to successively reduce the values of n_{eff} and therewith δn_{eff}. For as-proton-exchanged layers and low modes propagating close to the surface, δn_{eff} is larger than 0.07, and r_{333} is almost zero. Annealing at a temperature of 400 °C and for a total time of 320 min leads to $\delta n_{\mathrm{eff}} < 0.03$, and the coefficient r_{333} is nearly completely recovered to the bulk value. Alternative techniques for electro-optic coefficient measurements based on interferometric methods [39, 81] and modulation of the reflection pattern from the sample surface [65, 82] have been reported.

In channel waveguides, the electro-optically induced phase changes in integrated Mach–Zehnder [38, 40] or Fabry–Pérot interferometers [83] have been used to measure electro-optic coefficients in LiNbO$_3$ and LiTaO$_3$ samples.

2.3 Holographic methods

Photorefractive effects in planar waveguides can be studied by two principal holographic methods, namely by utilizing a two-beam interference setup, or by monitoring the output intensity and the beam shape of a single guided beam. In particular in the former case, a wide variety of holographic measurement techniques [84] for material characterization can be applied. In channel waveguides light-induced phase changes can be measured interferometrically in the same way as electro-optic effects, i.e., by a non-holographic method. Here pump probe techniques are often utilized, where a low-power beam of larger wavelength that does not cause photorefractive effects itself, is used to measure refractive index changes. In the following, some investigation methods for planar waveguides will be briefly described, and the expressions for usual measures for the size of photorefractive effects are given.

Light can be coupled into planar waveguides with the help of prisms or by direct endface coupling. Grating couplers may

be used as well, but fabrication is difficult and coupling efficiencies are low. On the one hand, prism coupling may be preferred for the investigation of multimode waveguides as it enables excitation of certain modes with well-defined intensity distribution, and thus depth-dependent measurements of waveguide properties become possible. On the other hand, endface coupling is of particular interest for waveguides in BaTiO$_3$, KNbO$_3$, or SBN, because sample dimensions are ususally too small to use a two-prism setup, and for some materials stress that is inherent in the prism–waveguide coupler may be not applied to the samples because of the risk of depoling of the single-domain crystals.

Elementary refractive index gratings can be written by two guided beams intersecting inside the waveguide [85]. In general, both beams have the same polarization and mode number, and they intersect under a certain angle, but gratings can be recorded with different modes, orthogonal polarization, or in a linear geometry, too [12, 86]. Furthermore, gratings may be written by external beams that impinge upon the surface of the waveguiding layer [87, 88]. The readout of gratings is possible by shortly blocking one of the writing beams; alternatively another beam of different (longer) wavelength that is coupled in under the corresponding Bragg angle may be used for continuous reading.

The temporal development of the *refractive index modulation* Δn during writing and decay of the grating can be described by exponential laws [89],

$$\Delta n(t) = \Delta n_{\mathrm{s}} \left[1 - \exp\left(-t/\tau\right) \right] , \tag{2}$$

$$\Delta n(t) = \Delta n_{\mathrm{s}} \exp\left(-t/\tau\right) . \tag{3}$$

Here Δn_{s} is the refractive index change in saturation, and τ is the grating buildup time or Maxwell time for holographic recording.

The *diffraction efficiency* η is defined as the ratio of diffracted and total transmitted light intensity. It is connected to the amplitude of the refractive index modulation and interaction length d via Kogelnik's equation [90],

$$\eta = \sin^2 \left(\frac{\Delta n \pi d}{\lambda \cos \Theta} \right) , \tag{4}$$

where λ is the vacuum wavelength of light and Θ is the angle at which the recording beams intersect in the waveguide.

The *holographic sensitivity* S can be expressed as the ratio of saturated refractive index change and the product of intensity I and grating buildup time τ,

$$S = \frac{\Delta n_{\mathrm{s}}}{I \tau} . \tag{5}$$

When the refractive index grating is not in phase (or antiphase) with the light intensity pattern, a signal beam I_{s} can be amplified by a pump beam I_{p}. The *logarithmic gain coefficient* Γ of this two-wave mixing is described by

$$\Gamma = \frac{1}{d} \ln \left(\frac{I_{\mathrm{s}} I_{\mathrm{p}}^{\mathrm{o}}}{I_{\mathrm{s}}^{\mathrm{o}} I_{\mathrm{p}}} \right) . \tag{6}$$

Here $I_{s,p}^o$ and $I_{s,p}$ are the light intensities of signal and pump wave at the beginning of the interaction and after the grating has been written until saturation, respectively. In the undepleted pump approximation, i.e., $I_p \approx I_p^o$, the signal wave is amplified exponentially, $I_s = I_s^o \exp(\Gamma d)$.

In most investigations of photorefractive waveguides averaged quantities have been used to describe both the light distribution inside the sample and the photorefractive properties, for example, effective widths and propagation depths of the excited modes, averaged light intensities, or refractive index changes and photovoltaic constants where the values are averaged over the depth of the waveguiding layer [91]. For these averaged quantities the Kogelnik theory of the interaction of plane waves may be used to interpret the results. However, in some cases the simplified treatment of the interacting beams as plane waves has failed to describe the experimental observations. For a more accurate evaluation of the measurements the two-dimensional intensity distribution has to be taken into account. For example, the two-wave interaction of Gaussian beams inside a waveguiding layer can be interpreted in terms of a spatially varying time constant for the grating buildup time that is smallest in the beam center and increases towards the sides of the Gaussian profile [92]. Furthermore, the two-dimensional shape of the intensity distribution has to be considered in particular for those wave mixing experiments that depend critically on the small thickness of the waveguiding layer [93, 94], i.e., for interactions that have no analogs in bulk samples.

When only a single beam is coupled into the planar photorefractive waveguide, both, light-induced phase changes in the beam path and holographic scattering reduce the transmitted power in the beam direction [95, 96]. Photoconductivity, refractive index changes, and holographic sensitivity can be quantitatively determined by input power and time dependent measurements of the resulting changes in the shape of the out-coupled intensity spectrum [97].

3 Materials

In this section, the properties of photorefractive planar and channel waveguides in different materials, including $LiNbO_3$, $LiTaO_3$, $BaTiO_3$, $KNbO_3$, SBN, and crystals of the sillenite type (BSO, BTO, BGO), will be discussed.

3.1 Lithium niobate

Among all the electro-optic materials photorefractive effects have been studied most extensively in lithium niobate ($LiNbO_3$) [2]. Very large crystals with diameters up to four inches and of superior optical quality can be grown. $LiNbO_3$ has rather high electro-optic and SHG coefficients of $r_{333} \approx 30\,pm/V$ and $d_{333} \approx 32\,pm/V$, respectively. The crucial influence of transition metal dopants, for example, iron or copper, on the photorefractive properties was discovered very early. Today the charge transport in $LiNbO_3$ bulk samples is well understood for cw as well as for pulse laser intensities [98]. Both, photorefractive sensitivity and refractive index changes of doped crystals are high. However, when compared to other ferroelectric crystals such as the perovskites $BaTiO_3$ and $KNbO_3$, or SBN, photoconductivity is

at least two or three orders of magnitude lower. Thus typical recording times of refractive index gratings in the bulk are in the range of minutes. On the other hand, $LiNbO_3$ has been intensively investigated as holographic storage material because of the low dark conductivity that enables storage times up to years.

By far the most of the published fundamental and applied work on photorefractive properties of waveguides has been done by using $LiNbO_3$, mainly because of the large interest in this crystal for its use as a substrate material in integrated optics. Advantages of $LiNbO_3$ are the easy formation of high-quality low-loss waveguides, chemical and mechanical resistance, a wide range of nonlinear optical interactions, and finally the availability of good and large crystals at a reasonable cost. Most of the available literature on photorefractive $LiNbO_3$ waveguides, starting with the first reported photorefractive effects in 1975 [85, 99] and up to the year 1986, is reviewed in [6]. In the meantime new photorefractive effects in $LiNbO_3$ waveguides have been found, and improved theoretical descriptions have enabled a better understanding of the involved mechanisms. The following sections will concentrate on these recent investigations of planar and channel waveguides in $LiNbO_3$.

3.1.1 Planar waveguides. Light-induced refractive index changes in an optical material can be considered from two points of view. On the one hand, these photorefractive effects are of considerable interest for applications in holographic storage and optical communication technology. On the other hand, the same mechanism is feared as optical damage; for example, in waveguide devices light-induced phase shifts may degrade the optical performance.

Optical damage resistance of planar $LiNbO_3$ waveguides fabricated by different technologies has recently been investigated by various groups. In Table 1 some values of steady-state refractive index changes and holographic sensitivity for waveguides prepared by different techniques are summarized. However, only values measured at similar light intensities may be compared. In general, steady-state refractive index changes, holographic sensitivity, and photoconductivity depend on light intensity [100, 101]. For certain fabrication methods, dark conductivity of the waveguiding layer is considerably enlarged, and particularly at higher light intensities more than one photorefractive center can be involved in the charge transport mechanism [102], thus making the above quantities intensity dependent.

Furthermore, the impurity level of the used substrate material as well as impurities that are incorporated by the waveguide fabrication itself, play an important role for the photorefractive behavior of the investigated samples; but in most published work on optical damage in $LiNbO_3$ waveguides the concentration of impurities has not been measured. Therefore, the results given in Table 1 should only be regarded as a general tendency of the size of photorefractive effects in different types of waveguides.

A high holographic sensitivity and large light-induced refractive index changes have been found for titanium-diffused samples [97]. It has been recognized that Fe^{2+} centers are stabilized by Ti^{4+} ions against oxidation [91], thus increasing the sensitivity to optical damage considerably.

Much higher photorefractive damage resistance has been obtained for waveguides prepared by diffusion of zinc into

Table 1. Saturated refractive index change Δn_s and photorefractive sensitivity S at intensity level I for different planar z-cut waveguides in lithium niobate. Wavelength is 632.8 nm. TI, titanium-indiffused; PE, proton-exchanged; APE, annealed proton-exchanged; LPE:B and LPE:V, liquid phase epitaxy with $Li_2O-B_2O_3$ and $Li_2O-V_2O_5$ flux, respectively

Substrate	Type	Polarization	Δn_s	$S/cm^2/J$	$I/W/cm^2$	Reference
LiNbO$_3$	TI	TE	2×10^{-4}	4×10^{-7}	10^3	[97]
		TM	6×10^{-4}	9×10^{-6}	10^3	
	PE	TM	1×10^{-5}	2×10^{-11}	10^3	
	APE	TM	2×10^{-4}	3×10^{-9}	10^3	
LiNbO$_3$:MgO	LPE:B	TE	2×10^{-5}	2×10^{-8}	10^3	[97]
	LPE:V	TE	3×10^{-4}	9×10^{-8}	10^3	
LiNbO$_3$	PE	TM	4.2×10^{-6}	3.8×10^{-12}	1.3×10^4	[103]
	APE	TM	5.1×10^{-6}	5×10^{-9}	2.2×10^2	
LiNbO$_3$:7%MgO	PE	TM	4.9×10^{-6}	1.8×10^{-11}	1.8×10^4	[103]
	APE	TM	5×10^{-6}	1.4×10^{-8}	10^2	

LiNbO$_3$ [18]. In these samples no photorefractive effects have been observed for light intensities up to $90\,kW/cm^2$.

Proton exchange leads to lower values of holographic sensitivity both for annealed (APE) and non-annealed (PE) samples [97, 103] when compared with titanium diffusion. In strongly exchanged waveguides no light-induced refractive index changes for cw and pulse laser intensities ($I_{cw} \leq 5\,kW/cm^2$, $I_{pulse} \leq 5 \times 10^8\,W/cm^2$) have been measured [104], and this effect has been attributed to both a large increase of dark and photoconductivity [100] and a strong degradation of the electro-optic properties [36]. Furthermore, a conversion of Fe^{2+} to Fe^{3+} has been found for the PE process [105], which can explain the observed decrease in holographic sensitivity, too.

Annealing treatment of PE layers leads to a recovery of the electro-optic coefficients [40], while at the same time photoconductivity only slightly decreases [100]. Although the holographic sensitivity of APE samples is thus increased with annealing time, it is still two orders of magnitude lower than for titanium-indiffused samples. The use of MgO-doped LiNbO$_3$ substrates for proton exchange has resulted in only slightly enlarged photorefractive damage resistance [103].

Planar waveguides fabricated by liquid phase epitaxy (LPE) [106] have shown higher holographic sensitivity than PE samples, but the values are still lower than for titanium diffusion [97, 107]. The lowest values have been obtained for samples grown by using $Li_2O-B_2O_3$ flux, and when compared to proton exchange, no degradation of the electro-optic properties was measured. Other methods of thin film deposition have recently been used to grow epitaxial LiNbO$_3$ layers, for example, sputtering [108, 109], the sol-gel process [110], and pulsed laser deposition (PLD) [62, 111], but the photorefractive properties of these samples have not yet been reported.

Quite a few optical wave mixing experiments have been performed in planar LiNbO$_3$ waveguides, and most of the used samples were treated to enhance the photorefractive effects, for example, by iron or copper indiffusion, or combined proton and copper exchange. The published work may be subdivided into isotropic wave mixing, where the interacting light beams have the same polarization, and anisotropic wave mixing, where orthogonally polarized modes interact. In the following, new results of both isotropic and anisotropic wave mixing will be reviewed.

In contrast to wave mixing in the bulk where elementary refractive index gratings are usually recorded utilizing plane waves, in waveguides the inhomogeneity of the interacting fields and the presence of different modes have to be taken into account [93, 112]. As a result, several photorefractive processes have been identified in waveguides that have no true analogs in volume crystals, for example, polarization conversion of copropagating TE and TM modes [113], or the recording of gratings where the photovoltaic current is directed perpendicular to the grating vector [94].

In multimode planar waveguides, light can be scattered under discrete angles from an excited mode into other modes with different mode indices, but with the same polarization. In this interaction the pump and the scattered waves have to fulfill a corresponding phase matching condition, and the stray light can be amplified by parametric interaction. Because light waves that belong to different modes of the waveguide are involved in this type of wave mixing, the interaction is called parametric intermode scattering [12, 114–116].

An example of parametric intermode scattering is illustrated in the wave vector diagram of Fig. 4. In the planar waveguide a mode with index m propagating with the wave vector k_m in the x direction is excited. In general, some intensity is uniformly scattered in the m lines of both the excited and the other modes of the waveguide [95]. However, under certain discrete, symmetric angles relative to the x direction and for modes with a lower mode index, i.e., a higher effective refractive index and thus a larger wave vector, a parametric interaction of the excited wave k_m and a pair of scattered waves $k_{m-n}^{l,r}$, $n = 1, 2, \dots$ becomes possible. Here the indices
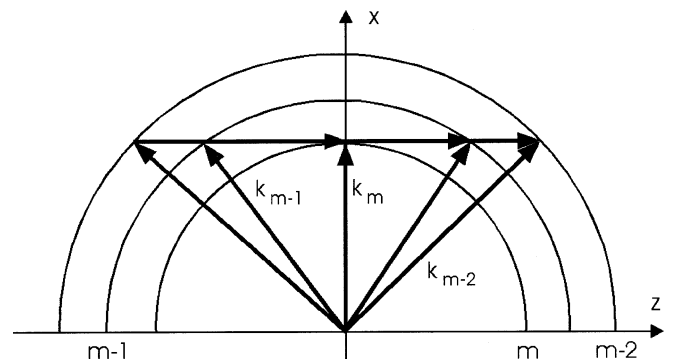
Fig. 4. Wave vector diagram of parametric intermode scattering in planar LiNbO$_3$ waveguides. Here k_m and m are wave vector and mode index of TE_m mode, respectively

l and r describe the waves scattered to the left and right, respectively. In the case considered here the three waves fulfill the phase matching condition $K = k_m - k_{m-n}^l = k_{m-n}^r - k_m$. The refractive index grating K is written by the pump wave k_m and the wave scattered to the left, k_{m-n}^l, as well as by the wave scattered to the right, k_{m-n}^r, and the pump wave k_m. Thus both scattered waves are amplified parametrically at the expense of the pump wave.

Different types of parametric intermode scattering in Fe- and Cu-doped LiNbO$_3$:Ti waveguides have been identified [12], including the interaction of leaky modes [115]. The amplification of weak signal beams by parametric interaction has been studied both theoretically and experimentally [114, 117, 118], and this has allowed the determination of material parameters describing the photorefractive properties of the investigated samples. A peculiarity of intermode scattering is the generation of subharmonic gratings [116]. The excitation of a third wave of mode m in the x direction by two pump beams of mode $(m-1)$ that propagate under symmetric angles relative to the new wave has been demonstrated. The two pump waves write a grating with grating vector K, and both pump waves are simultaneously diffracted in the direction of the signal wave by a grating with a grating vector $K/2$.

Up to now, the parametric interactions described above have only been observed for light of the same polarization, for example, either for TE or for TM modes; however, the anisotropic analog, where pump and stray light are polarized orthogonally to each other, should exist in principle, too. In other experiments, an interaction of this type has been found for copropagating TE and TM modes, i.e., in contrast to the intermode scattering shown in Fig. 4 in this interaction the grating vector is in the direction of light propagation. In the following a brief description of this process will be given.

In LiNbO$_3$ (as well as in LiTaO$_3$) waveguides, orthogonally polarized modes can write holographic gratings via photovoltaic currents, enabling strong beam coupling [113] and the generation of phase-conjugate [17] waves. The pump waves are orthogonally polarized with respect to the signal and phase-conjugated waves, respectively, and thus the interaction is called frequency-degenerate anisotropic wave mixing. This interaction, also known as polarization conversion, was first observed in 1981 in channel waveguides [119]. A detailed discussion of polarization conversion effects in LiNbO$_3$ channel waveguides can be found in [6]. Here we will concentrate on the corresponding process in planar waveguides, which was observed some years later in strongly iron-doped LiNbO$_3$ waveguides [120].

The redistribution of photoexcited charge carriers in LiNbO$_3$ (and LiTaO$_3$) crystals is mainly caused by the photovoltaic effect. Following from a phenomenological theory [121], the polarization-dependent photovoltaic current density is given by

$$j_k = \sum_{l,m} \left(\beta_{klm}^s + i\beta_{klm}^a \right) E_l^* E_m . \tag{7}$$

Here $\beta^{s,a}$ are the real linear and circular components of the photovoltaic tensor, and $E_{l,m}$ are the interacting light fields. For two copropagating orthogonally polarized light waves, a photovoltaic current is excited that is proportional to the non-diagonal tensor element $\beta_{131} = \beta_{232}$. This current is modulated with the grating period $\Lambda = \lambda/(n_o - n_e)$, where λ is the light wavelength in vacuum and $n_{o,e}$ are ordinary and extraordinary refractive indices.

The photovoltaic current causes the buildup of a periodic space charge field E_k, which leads to a perturbation of the dielectric tensor via the electro-optic effect,

$$\Delta\varepsilon_{ij} = -\varepsilon_{is} r_{stk} E_k \varepsilon_{tj} , \tag{8}$$

where r_{stk} is the electro-optic tensor component. The perturbation $\Delta\varepsilon$ has a local contribution according to β^s and a nonlocal part according to β^a [122]. As is well known, the shifted (nonlocal) grating leads to an energy exchange between the two interacting beams that depends on the sign of β^a. For iron-doped LiNbO$_3$ ordinarily polarized light is converted to extraordinary polarization.

We have shown that the amplitude of the space charge field depends on the ratio of grating period Λ and the width of the light distribution in the direction of the photovoltaic current [86]. In y- and z-cut channel waveguides, and also in y-cut planar waveguides, the waveguide thickness, which defines the lateral dimension of the light distribution, is comparable to the grating period Λ, which is about $6\,\mu m$ for LiNbO$_3$. This results in a non-vanishing space charge field [123], and orthogonally polarized modes can exchange intensity [113, 120, 124]. In planar z-cut waveguides, the beam width (aperture) of the excited mode is usually much larger than the grating period, thus no, or only small, mode coupling is expected. For counterpropagating orthogonally polarized modes, the grating period $\Lambda = \lambda/(n_o + n_e)$ is of the order of some tens of nm. Now Λ is small compared to the dimensions of the waveguiding structures, and the space charge field vanishes in channel waveguides and y-cut planar waveguides, too.

Examples of anisotropic wave mixing in planar LiNbO$_3$: Ti:Fe waveguides are given in Fig. 5. In Fig. 5a we show the intensity distributions of anisotropically diffracted stray light for excitation of ordinarily polarized light [86]. For y-cut waveguides, the maximum of TE-polarized light is in the direction of the excited TM mode, indicating strong coupling of copropagating waves. In z-cut waveguides, two maxima of TM-polarized amplified light at symmetric angles are observed, whereas in the propagation direction the intensity, i.e., anisotropic coupling, is nearly zero. In this case the beam width is 0.4 mm, which is much larger than the grating period Λ. Figure 5b shows the strong coupling and anisotropic diffraction of two excited TE and TM modes copropagating in a y-cut waveguide [17]. When both beams are switched on, energy is transferred from the TM to the TE mode, and when the TE mode is switched off, the TM light is anisotropically diffracted until the grating is erased. Using anisotropic beam coupling we have been able to determine the size of non-diagonal photovoltaic tensor elements $\beta_{131}^{s,a}$ as a function of experimental parameters [86, 125]. Alternatively, Raman microprobe characterization has been used for the measurement of $\beta_{131}^{s,a}$ [126].

3.1.2 Channel waveguides.

Different kinds of channel waveguides in nominally pure and MgO-doped LiNbO$_3$ have been formed by titanium indiffusion, PE and APE, and ion implantation. Photorefractive properties of these waveguides have
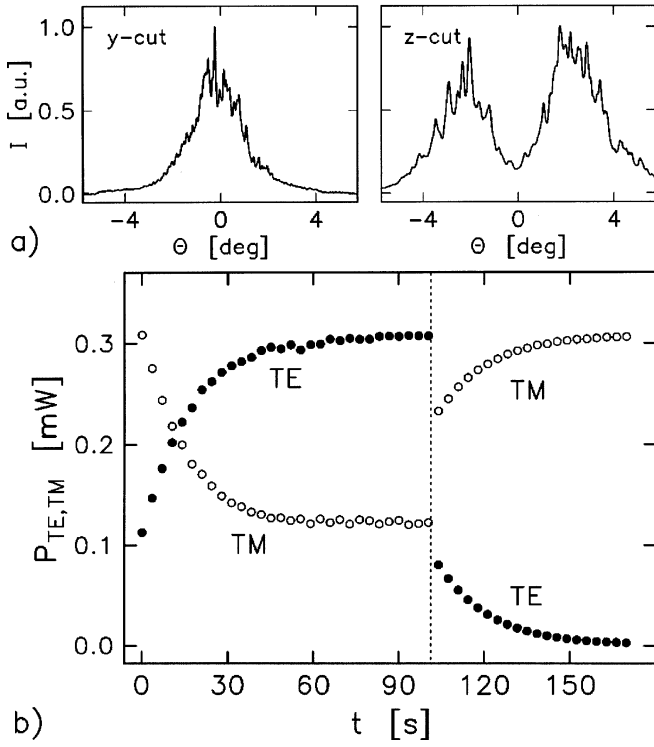
Fig. 5a,b. Anisotropic wave mixing in planar LiNbO$_3$:Ti:Fe waveguides [17, 86]. **a** Angular distribution of extraordinarily polarized stray light intensity in y- and z-cut samples, respectively, for the excitation of ordinarily polarized waveguide modes. The angle Θ is measured inside the sample relative to the x direction, that is the propagation direction. **b** Anisotropic beam coupling of a TE and a TM mode in a y-cut sample. The TE mode is amplified by the TM mode. At $t = 100$ s the TE mode is switched off, and the TM light is anisotropically diffracted until the grating is erased

ther enlarged conductivity in the APE samples, too. However, for higher intensities of some kW/cm^2 the differences of the refractive index changes in samples fabricated by different techniques decrease because of saturation, i.e., in all cases the refractive index changes tend to a maximum value of some 10^{-4}.

The use of LiNbO$_3$ doped with MgO has reduced refractive index changes in APE channel waveguides by nearly two orders of magnitude at intensities of some kW/cm^2 [130], and photoconductivity has been decreased at the same time, too. It has been concluded that strongly reduced photovoltaic currents in LiNbO$_3$:MgO waveguides are responsible for this effect. However, the observed behavior of photoconductivity is different when compared with both LiNbO$_3$ bulk crystals and planar waveguides, where photoconductivity is increased by magnesium doping [103]. Furthermore, for bulk LiNbO$_3$:MgO no dependence of photovoltaic currents on magnesium doping has been observed [98].

Implantation of H$^+$ into LiNbO$_3$ with subsequent annealing treatment has resulted in waveguides with strong light-induced refractive index changes [131] that are larger than for APE waveguides and almost comparable with titanium-diffused samples. At the same time, both dark and photoconductivity are at least as high as for APE waveguides. On the other hand, strongly reduced optical damage has been found for a combination of proton exchange and ion implantation, when APE waveguides are additionally implanted with 1-MeV H$^+$ through the existing waveguide channels [132].

In a more recent work, light-induced shifts in the phase matching curve of second-harmonic generation in both single-domain and domain-inverted LiNbO$_3$ channel waveguides have been investigated by using a pump probe technique [133]. A high photorefractive sensitivity connected with a two-step two-photon excitation has been found for single-domain samples, whereas optical damage was strongly reduced for domain-inverted samples.

recently been reported in several papers, and some of the results are listed in Table 2.

Fujiwara et al. have compared the photorefractive properties of titanium-diffused, PE, and APE samples using an integrated Mach–Zehnder interferometer [127–129]. For low intensities of some W/cm^2, saturated refractive index changes of titanium-diffused samples are about three orders of magnitude larger than in PE, and two orders of magnitude larger than in APE waveguides. This may be attributed to the large increase of dark conductivity for the PE and APE samples [129], and partly reduced electro-optic coefficients of the PE waveguides. Furthermore, holographic sensitivity is increased by a factor of four for APE waveguides [128] when compared with PE waveguides, mainly because of the restored electro-optic properties, and probably because of a fur-

3.1.3 Fiber-like crystals. Photorefractive single-domain fiber-like LiNbO$_3$ crystals have been grown by the resistance- and laser-heated pedestal growth method [134–136]. Angular-multiplexed holographic recording has been obtained in 3-mm-long rods with diameters of 0.2 and 0.5 mm [134, 135]. In these investigations intrasignal coupling, i.e., interaction of different spatial components of the signal beam, was avoided by utilizing a phase conjugating mirror for the reconstruction of the stored images [135]. Furthermore, narrow-bandwidth, electro-optically tunable holographic reflection filters written in a 12-mm-long sample with a very low spectral width of 0.02 nm have been demonstrated [136].

Table 2. Saturated refractive index change Δn_s and photorefractive sensitivity S at intensity level I for different z-cut channel waveguides in lithium niobate. Wavelength is 632.8 nm. TI, titanium-indiffused; PE, proton-exchanged; APE, annealed proton-exchanged

Substrate	Type	Polarization	Δn_s	S/cm^2/J	I/W/cm^2	Reference
LiNbO$_3$	TI	TE		2×10^{-7}	1	[127]
		TM	1.1×10^{-4}	6×10^{-7}	1	
LiNbO$_3$	PE	TM	8×10^{-6}	5×10^{-10}	10^2 ($\lambda = 488$ nm)	[128]
	APE	TM	5.3×10^{-5}	2×10^{-9}	10^2 ($\lambda = 488$ nm)	
LiNbO$_3$	APE	TM	4×10^{-4}	1.3×10^{-7}	10^4	[130]
LiNbO$_3$:7%MgO	APE	TM	1×10^{-5}	6×10^{-7}	10^4	[130]

3.2 Lithium tantalate

Lithium tantalate (LiTaO$_3$) has electro-optic, nonlinear optical and photorefractive properties similar to LiNbO$_3$. On the one hand, in some aspects LiTaO$_3$ is an even more attractive material for applications to integrated optics than LiNbO$_3$. At a constant light wavelength in the blue/green spectral region, the former is less susceptible to optical damage, is more transparent in the near ultraviolet, has a smaller, positive birefringence, and it has even better mechanical properties. On the other hand, waveguide formation is more difficult, as necessary temperatures for diffusion of metals into LiTaO$_3$ exceed the Curie temperature of about 620 °C, and the difficult crystal growth at the very high melting point of LiTaO$_3$ of about 1650 °C limits the commercial availability of large crystals with a good optical quality.

Planar and channel LiTaO$_3$ waveguides have been fabricated by diffusion of, for example, titanium [11], niobium [19], or zinc [83], as well as by proton exchange [25, 31, 137]. Alternative low-temperature techniques are copper exchange in molten inorganic copper salts [44], or non-isovalent exchange of metal ions (Me^{2+}) for two single-charged lithium ions [138]. After diffusion above the Curie temperature repoling of the samples is necessary to recover the electro-optic properties of LiTaO$_3$. In most work on proton-exchanged LiTaO$_3$ waveguides, electro-optic coefficients have been found to be strongly decreased after the exchange, and the values were at least partially restored after additional annealing treatment [39, 81].

Optical damage effects in zinc-diffused LiTaO$_3$ channel waveguides have been investigated in [139], and refractive index changes of $\Delta n_e \approx 5 \times 10^{-5}$ at a wavelength of 488 nm and an intensity of 1 kW/cm^2 have been measured. Proton-exchanged planar LiTaO$_3$ waveguides have shown similar refractive index changes of about 4×10^{-5} [140], but at a larger wavelength of 632.8 nm. The temperature dependence of photorefractive effects in PE waveguides has been investigated in [140].

Since the early work of Wood et al. [85], only in a few recent papers wave mixing in LiTaO$_3$ waveguides has been reported. We have used anisotropic two- and four-wave mixing to determine the photorefractive properties of titanium-diffused LiTaO$_3$:Ti:Fe waveguides [141]. In these samples, phase-conjugate efficiencies up to 9% have been achieved. In a more recent work [42], we have fabricated photorefractive LiTaO$_3$ waveguides by combined proton and copper exchange at low temperatures, thus avoiding necessary repoling of the samples. The photorefractive efficiency has been considerably increased by the additional copper exchange [142]. As an example, the intensity dependence of steady-state diffraction efficiency for samples with different copper doping is illustrated in Fig. 6. Here all samples were annealed for 1 h after the ion exchange. Further annealing treatment results in a full recovery of the α-phase of LiTaO$_3$ [42], and diffraction efficiencies up to 81% have been achieved when we annealed the samples for 16 h [143].

Thin epitaxial LiTaO$_3$ films have been grown by different methods, and research has been stimulated again recently by the large interest in LiTaO$_3$ waveguides with domain-inverted structures for second-harmonic generation. An overview of published work can be found in [71]. However, very little is known about the optical and nonlinear properties of
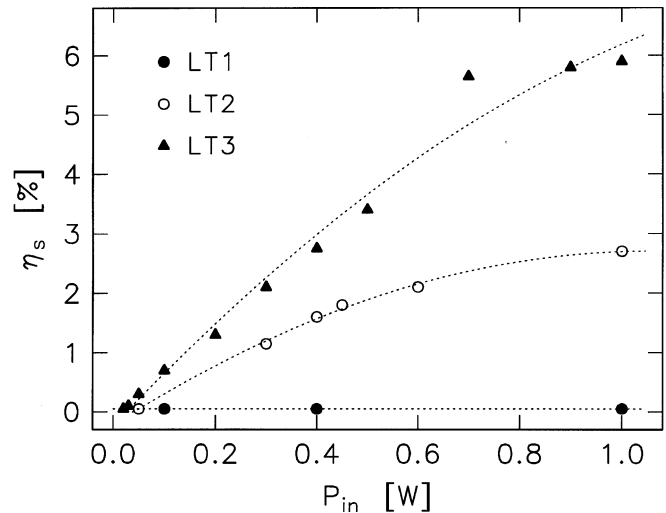
Fig. 6. Steady-state diffraction efficiency η_s as a function of input power P_{in} (wavelength 488 nm) for different planar LiTaO$_3$:H:Cu waveguides fabricated by combined proton and copper exchange [42]. LT1, undoped proton-exchanged waveguide; LT2, additionally copper-doped; LT3, copper concentration is about 2.3 times that of sample LT2

these samples. Laser-deposited LiTaO$_3$ films on gallium arsenide substrates [144] may be of considerable interest because they allow for the development of integrated optical devices with laser sources, frequency doublers, and photodiodes. Waveguiding has been observed for LiTaO$_3$ layers on sapphire [145] and silicon [146] substrates, fabricated by PLD, too. Furthermore, metal organic chemical vapor deposited (MOCVD) films on sapphire have shown high SHG coefficients up to 12 pm/V after electric field poling [71].
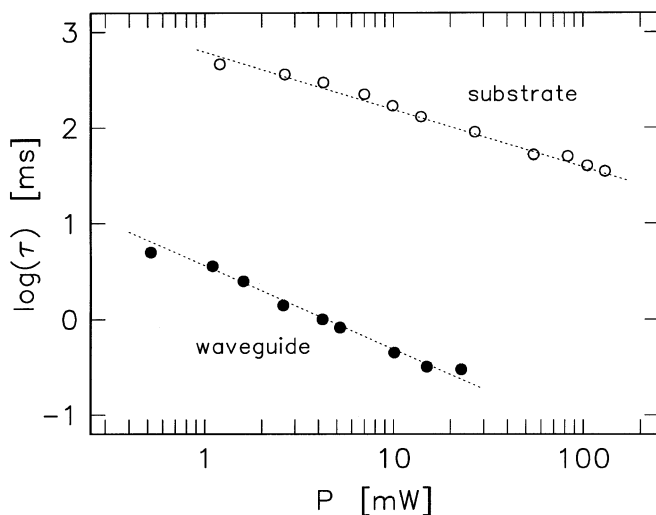
3.3 Barium titanate

Photorefractive barium titanate (BaTiO$_3$) crystals are currently used for a wide range of nonlinear optical applications [2]. Amplification of weak optical beams by more than three orders of magnitude in a two-beam coupling experiment [147] and self-pumped phase conjugation with efficiencies up to 80% [148] in the near IR have been demonstrated. The enormous interest in this material may be due to its very large electro-optic coefficient $r_{131} = 1640$ pm/V, which is one of the largest values known for any material. However, the practical use of BaTiO$_3$ crystals is at least partly limited by the response time in optical wave mixing, which is indeed much smaller than for LiNbO$_3$ and LiTaO$_3$, but still too large for most applications. Obviously, a significant decrease in response time can be achieved by using planar BaTiO$_3$ waveguides, i.e., by making use of the high intensities inherent in waveguide geometries.

Planar optical waveguides in BaTiO$_3$ were first fabricated by Moretti et al. [47] in 1990 by implantation of 2-MeV He$^+$ at a dose of 10^{16} cm^{-2}. Both the ordinary and the extraordinary refractive index were decreased in the region of the implanted barrier [149], and the optical quality of the samples was well preserved with no noticeable increase of absorption by color centers as has been observed for LiNbO$_3$. As for other oxide crystals, it has been found that H$^+$ implantation into BaTiO$_3$ [49] can be used for waveguide formation, too.

Two-wave mixing in a 1.5-MeV H^+-implanted BaTiO$_3$ waveguide was reported by Youden et al. [150] in 1992. As can be seen in Fig. 7, the nearly 15-μm-thick waveguiding layer with an optical loss of 3.2 cm^{-1} showed a decrease of response time of about two orders of magnitude when compared to the same input power in the substrate. This is mainly related to the better optical confinement in the waveguide. However, the beam coupling direction was reversed to that of the substrate, which can probably be attributed to a change in the dominant charge carrier species from holes to electrons because of electrochemical reduction of impurities by the ion beam. A possible reversal of the direction of ferroelectric domains, which is due to heating of the sample surface during implantation, may be considered as well. Both self-pumped phase conjugation [151] and mutually pumped phase conjugation [152] in the same sample have been obtained, too.

Recently, single-domain tetragonal fiber-like BaTiO$_3$ crystals have been grown by the laser-heated pedestal growth method [153]. The photorefractive behavior of these samples has been investigated by beam coupling and holographic image storage; however, refractive index changes are low when compared with the properties of the bulk.

Motivated by the great interest in ferroelectric thin film fabrication for application in VLSI technology and nonlinear optics, large efforts have been made in the fabrication of epitaxial BaTiO$_3$ layers. A variety of deposition techniques has successfully been used for the formation of BaTiO$_3$ thin films on adequate substrates, for example, MBE [67], the sol-gel process [73], MOCVD [70], or PLD [154]. Up to now only little information on the optical properties of these layers is available. Channel waveguides synthesized by MOCVD and additional etching in an HF solution have shown moderate optical loss of 1 to 2 cm^{-1} at 1.55 μm [155] and effective electro-optic coefficients of about 50 pm/V [156]. Electro-optic coefficients that are strongly reduced in comparison to data for the bulk have been reported for nominally pure and cerium-doped BaTiO$_3$ polycrystalline films fabricated by

PLD [157]. Recently, epitaxial and very smooth films have been fabricated by the technique of pulsed laser deposition combined with in situ annealing of the growing film [63, 158], and future improvement and investigation of the nonlinear properties of these films may be of great promise.
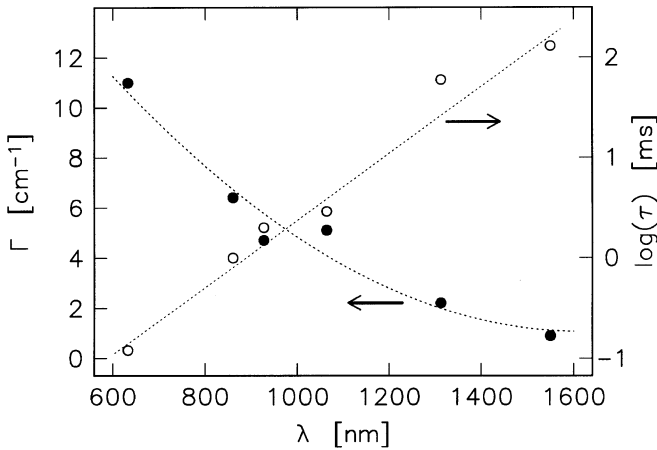
3.4 Potassium niobate

Among the most promising ferroelectric oxides, potassium niobate (KNbO$_3$) has been shown to have excellent electro-optic, nonlinear optical, and photorefractive properties [159]. High nonlinear and electro-optic coefficients in the spectral range of diode lasers, and a high photorefractive sensitivity, which can be extended to telecommunication wavelengths by additional doping, have been reported. This makes the crystal a particularly attractive candidate for applications in integrated optics, such as intensity modulators with low half-wave voltage, second-harmonic generation for cheap blue/green laser sources, or optical switching and modifiable interconnections.

Methods of waveguide formation that have been successfully applied to other materials such as diffusion or ion exchange have been found to be not applicable to KNbO$_3$, probably because of the densely packed lattice of the perovskite structure. The first permanent waveguides in KNbO$_3$ were realized by implantation of He$^+$ in 1988 by Bremer et al. [48]. Low-loss planar waveguides with damping coefficients of about 1 cm^{-1} (wavelength 632.8 nm) can be formed by He$^+$ implantation at low doses of some 10^{14} cm^{-2} [160]. Even lower propagation loss of only 0.2 cm^{-1} has been found for a slightly higher dose of 1.5×10^{15} cm^{-2} [54]. For H$^+$ implantation doses of 10^{16} cm^{-2} and higher are used to produce good optical waveguides; here damping coefficients of 1 to 3 cm^{-1} for visible light have been reported [161, 162].

Channel waveguides in KNbO$_3$ with damping coefficients as low as 0.3 cm^{-1} for red light have been realized by Fluck et al. [59, 163] by repeated He$^+$ implantation. In addition to the formation of a planar waveguide by single energy implantation of the whole surface, side walls that define the waveguiding channels have been formed by multiple energy implantation through a thick mask. The possibility of fabricating non-leaky channel waveguides by ultralow dose implantation that leads to an increase of the refractive index of the implanted area has been demonstrated, too [58].

Two-wave mixing experiments have been performed to characterize the photorefractive properties of ion-implanted planar waveguides in KNbO$_3$. Both H$^+$ and He$^+$ implantation as well as nominally pure and iron-doped substrate crystals have been used. In all published work, the beam coupling direction in the implanted waveguides in KNbO$_3$ was reversed to that of the substrate [164]. For green light (wavelength 514.5 nm) and a waveguiding layer of about 6 μm thickness fabricated by H$^+$ implantation in KNbO$_3$:Fe, very high logarithmic gain coefficients up to 40 cm^{-1} have been obtained [161]. An example that demonstrates beam coupling at telecommunication wavelengths in a thicker, 3.5 MeV H$^+$-implanted KNbO$_3$:Fe waveguide is shown in Fig. 8. At a wavelength of 1.3 μm a logarithmic gain coefficient of 2.2 cm^{-1} with a response time of 60 ms for a pump power of about 4 mW was measured [162]. In this work, the photorefractive properties of the waveguide were found to be

Fig. 7. Beam-coupling in a H$^+$-implanted BaTiO$_3$ waveguide. Response time τ is measured as a function of the incident light power P (wavelength 488 nm) both for the waveguiding layer (●) and for the substrate (○). The beam area for bulk and waveguide differ by a factor of 1250, and the power in the waveguide is corrected for measured losses of 3.2 cm^{-1}. Data are taken from [150]

Fig. 8. Two-beam coupling in a H^+-implanted $KNbO_3$:Fe waveguide. Logarithmic gain coefficient Γ (●) and response time τ (○) are measured for different laser wavelengths and a pump intensity of $200\,W/cm^2$. The *dotted lines* are merely guides for the eye. Data are taken from [162]

favorably modified by H^+ implantation when compared to the bulk material. The photorefractive sensitivity is increased by approximately two orders of magnitude and extended to infrared wavelengths.

Several thin film deposition techniques have been used to fabricate single-crystal layers of $KNbO_3$ for applications in nonlinear optics. Films with a thickness of a few μm have been grown by LPE, producing waveguides that were multimode [165]. Thinner epitaxial $KNbO_3$ films formed by ion beam [166] and rf-diode sputtering [167] have shown interesting nonlinear properties; an SHG coefficient of $5\,pm/V$, which is one third of the bulk value, has been reported in [167]. Higher SHG coefficients of $13\,pm/V$ have been measured for epitaxial layers using MOCVD [72]. Promising results have been obtained for films using PLD and a potassium-enriched ceramic target [64, 168], too.

3.5 Strontium-barium niobate

Strontium-barium niobate crystals ($Sr_xBa_{1-x}Nb_2O_6$, $0.25 \leq x \leq 0.75$, SBN) can be grown in excellent optical quality. The most widely investigated crystal is that of the congruently melting composition, $x = 0.61$ (SBN61); other common compositions are $x = 0.5$ (SBN50) and $x = 0.75$ (SBN75). The crystals exhibit very large electro-optic coefficients, which are about ten times larger (SBN61) than those for $LiNbO_3$, and with suitable doping (for example, cerium, chromium, or rhodium) the photorefractive sensitivity is high. For this reason SBN permits many applications in optical data storage and processing [169, 170], and a lot of fundamental research has been done demonstrating the excellent photorefractive properties of this material [171–173]. Both channel and planar waveguide structures as well as single-crystalline fiber-like crystals have been realized in SBN. In the following the different types of waveguides and their optical and photorefractive properties will be discussed.

Planar and channel waveguide formation in SBN substrate crystals has been performed using sulphur [174] and zinc [175] indiffusion, but the achieved waveguides exhibit high losses greater than $2.5\,cm^{-1}$. He^+ implantation in SBN was first mentioned by Youden et al. [150] in 1992. A detailed investigation of the fabrication of planar SBN waveguides by H^+ and He^+ implantation followed in 1995 [51]. As a result, we have obtained low-loss waveguides ($0.35\,cm^{-1}$ for the wavelength 632.8 nm) for low-dose He^+ implantation or intermediate doses using H^+.

Two-wave mixing in cerium-doped SBN61 and SBN75 waveguides formed by H^+ implantation was demonstrated by Robertson et al. [176] in 1996. Later in 1997 we reported [177, 178] on the investigation of the photorefractive properties of planar optical waveguides in SBN61:Ce crystals, fabricated by H^+ and He^+ implantation. When compared to data for the bulk material at the same intensity, the response time for two-wave mixing in SBN waveguides is decreased by one or two orders of magnitude both for H^+ [176] and low-dose He^+ [177] implantation. It is not yet clear whether this effect is connected with an increase of dark conductivity, which we have observed for strongly H^+-implanted samples and high ion flux [51]. Another explanation may be the chemical reducing properties of the implanted ions, which lead to an increase of the concentration of filled traps [176], or the influence of additional photorefractive centers created by the implantation. The latter argument is confirmed by the observation that the photoconductivity σ_{ph} in our He^+-implanted layers depends nonlinearly on light intensity I, $\sigma_{ph} \propto I^x$, with an exponent $x \approx 0.55$ [177]. For the substrate material the photoconductivity is almost linear, and there the charge transport has been well explained by a one-center model with Ce^{3+}/Ce^{4+} as the photorefractive center [179].

With an increasing dose of implanted He^+ a decrease of two-wave mixing gain as well as of response time is observed [177], pointing to a strong degradation of the photorefractive properties for doses higher than $10^{15}\,cm^{-2}$.

The opposite effect has been found for H^+-implanted samples and the same range of ion doses [176]. This different behavior may be explained by the lower electronic and nuclear damage per ion for H^+ implantation, i.e., a higher "damage threshold" for the photorefractive properties at the same dose, and by the increase of dark conductivity already mentioned above.

Very high logarithmic gain coefficients of up to $45\,cm^{-1}$ with time constants of the order of ms have been obtained for extraordinarily polarized blue light, adequate cerium doping, and optimized implantation parameters [177]. For red and near infrared wavelengths these values are strongly reduced. As an example, in Fig. 9 the wavelength dependence of the logarithmic gain coefficient for two-wave mixing in a SBN61 waveguide and a He^+ dose of $10^{15}\,cm^{-2}$ is shown. It should be noted that in these samples [177] the direction of beam coupling may be reversed to that of the substrate when the sample is heated during the implantation process; but after the sample have been polarized again, the beam-coupling direction is the same as in the substrate.

Polycrystalline SBN thin films of various compositions have been obtained by LPE [69], rf sputtering [180], MOCVD [72], and the sol-gel process [74]. These films are preferentially orientated and show only reduced electro-optic coefficients [74], but no photorefractive properties have been reported. Epitaxial SBN61 [65, 181] and SBN75 [82] films on MgO substrates with very high electro-optic coefficients r_{333} of $380\,pm/V$ and $844\,pm/V$, respectively, have been fabricated by PLD, but only little is known about the optical
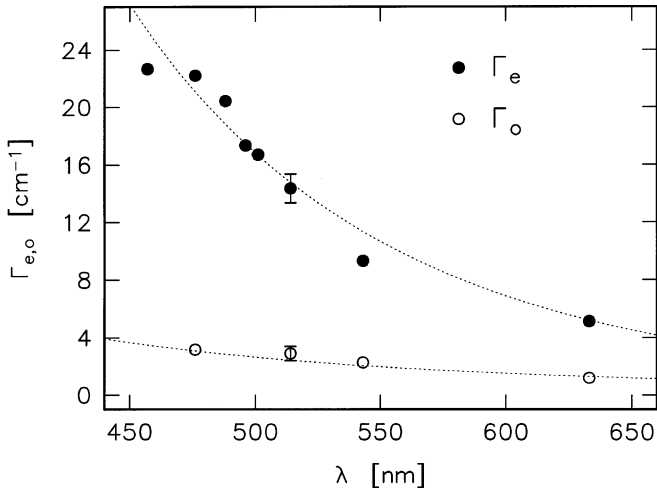
Fig. 9. Logarithmic gain coefficients $\Gamma_{e,o}$ for extraordinary ($\bullet$) and ordinary ($\circ$) light polarization measured for different wavelengths λ in a 2-MeV He$^+$-implanted SBN waveguide [177]. The *dotted lines* are merely guides for the eye

properties of such films [146]. The refractive indices of the fabricated layers [181] are about 3% lower than the values for the bulk [182]. However, together with other thin film deposition techniques PLD may be very interesting for future fabrication of photorefractive SBN waveguides, too.

Highly multimode single-crystalline fiber-like SBN crystals have been investigated by different groups using visible [183, 184] and near-infrared light [185]. Thin rods were grown from cerium-doped single-crystalline SBN61 with diameters ranging from 0.16 to 2 mm. Such samples have a high angular selectivity for multiplexed holographic recording because of multiple internal beam reflections and the long interaction length in two-wave mixing. Both, rods grown along the c axis of the crystal and those grown along the a axis were used in reflection and transmission geometry, respectively. The photorefractive properties are similar to those of the bulk crystal; but due to the higher light intensities in the fiber-like crystals typical grating formation times for μW input powers are in the range of some tens of ms [184]. Self-pumped phase conjugation has been observed in a sample where the c axis coincides with the rod axis [183], too.

Recently, channel waveguides in SBN have been fabricated by a refractive index increase because of the static strain-optic effect [186]. The strain is produced by a SiO$_2$ film deposited on the substrate surface at a temperature of 320 °C. Etching of small channels in this layer results in a waveguide with low propagation loss values of about 0.14 cm^{-1}. Fast electro-optic modulation up to 1 GHz for 1.3 μm wavelength has been demonstrated [187].

3.6 Sillenites

The crystals of the sillenite type, Bi$_{12}$SiO$_{20}$ (BSO), Bi$_{12}$TiO$_{20}$ (BTO), and Bi$_{12}$GeO$_{20}$ (BGO), have relatively small electro-optic coefficients, but photoconductivity and photorefractive sensitivity for visible and near-infrared light are high. These properties make the materials attractive candidates for real-time holography and optical phase conjugation.

Although optical waveguide fabrication in these materials has been reported in quite a few papers, very little is known

about the photorefractive properties of sillenite waveguides. Waveguiding has been observed in epitaxial BTO films fabricated by LPE on BGO substrates [188], as well as for PLD layers on single-crystalline zirconia [189] and sapphire [190]. For the latter electro-optical and nonlinear optical properties have been proved. Two-wave mixing in planar BTO waveguides grown on BGO substrates has been observed in [191]. The measured electro-optic coefficients as well as the beam coupling gain have been found to be almost two orders of magnitude lower when compared with the bulk material. A significant increase of the gain values has been obtained by applying an external electric AC field along the grating direction [192]. Furthermore, photorefractive single-crystalline fiber-like BSO and BTO crystals with lengths of several cm have been fabricated [193], and beam coupling in these fibers has been demonstrated.

3.7 Other materials

In some other photorefractive oxide crystals waveguiding layers have been formed by ion implantation. These materials include potassium-tantalate niobate (KTN), KTa$_{1-x}$Nb$_x$O$_3$, $0 \leq x \leq 1$ [194], and the tungsten-bronze-type crystal KNSBN, (K$_{0.5}$Na$_{0.5}$)$_{0.2}$ (Sr$_{0.75}$Ba$_{0.25}$)$_{0.9}$Nb$_2$O$_6$, [195]. Ferroelectric lead germanate (PGO), Pb$_5$Ge$_3$O$_{11}$, crystals have fairly large electro-optic coefficients of $r_{333} = 15.3$ pm/V and have proved to exhibit interesting photorefractive properties [196, 197]. Low-loss waveguides in this material have been fabricated by ion implantation [50], too. However, for all of the above materials photorefractive properties have not yet been investigated.

4 Applications

In the last two decades a large number of different optical components based on photorefractive waveguides have been proposed, and static (for example, narrow-bandwidth filters or multiplexers) and dynamic (for example, phase conjugators or modifiable interconnections) elements have been experimentally demonstrated. Corresponding to the various applications, quite different requirements for the properties of both waveguide and photorefractive parameters have to be fulfilled. In the following section, some of the applications of photorefractive waveguides will be presented, and their properties will be discussed.

4.1 Thermally fixed diffraction gratings

Permanent refractive index gratings in waveguide devices are of considerable interest for optical communication systems, for example, narrow-bandwidth mirrors for integrated waveguide lasers in LiNbO$_3$ [198, 199], or wavelength multiplexers that make use of the high spectral selectivity of holographic filters [200]. Other possible applications include grating couplers and sensor technology [87, 201].

Holographic gratings that are superimposed in a planar waveguide have been proposed for the separation of different wavelength channels [202, 203], and equivalent phase gratings in channel waveguides may be used together with optical
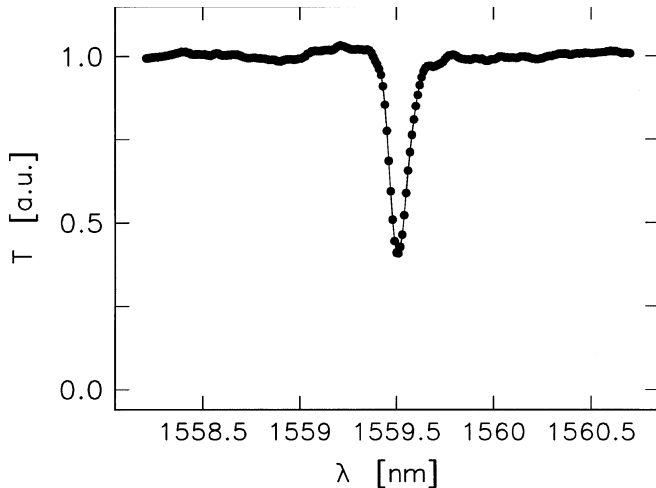
Fig. 10. Transmission spectrum $T(\lambda)$ of a thermally fixed holographic grating in a 15-mm-long LiNbO$_3$:Ti:Fe channel waveguide [207]. The reflectivity reaches 60% at a center wavelength of $\lambda = 1559.51$ nm, with a narrow bandwidth (FWHM) of 0.1 nm

N×N power dividers or in a cascading scheme. However, phase holograms in photorefractive crystals suffer from destructive readout when the material is illuminated with light of the recording wavelength. In order to avoid erasure, different methods have been developed to make the recorded holograms insensitive for the readout light. Interesting results have been obtained by electrical fixing [204], i.e., partial local reversal of ferroelectric domains, and in particular by the technique of thermal fixing [205]. Thermal fixing is performed by writing a holographic grating at elevated temperatures of about 180 °C. At these temperatures protons become mobile and compensate for the generated electronic space charge field [206]. After the sample has been cooled down, the illumination with incoherent light yields a quasi-stabilized fixed hologram.

Thermal fixing of holographic gratings has been investigated in both, planar [88] and channel LiNbO$_3$:Ti:Fe waveguides [199, 207]. High reflection efficiencies even for infrared light have been demonstrated. In Fig. 10, we illustrate the transmission spectrum of a thermally fixed reflection grating in a LiNbO$_3$:Ti:Fe single-mode channel waveguide [207]. The device was fabricated by recording a refractive index grating that is directed along the c axis of the sample with two external, ordinarily polarized writing beams of wavelength 514.5 nm utilizing a holographic setup. For readout of the grating, TE polarized light of a tunable DFB laser working around 1.55 μm is coupled into the 6-μm-wide channel. The filter has a peak reflectivity of 60% at a center wavelength of 1559.51 nm, and a bandwidth of 0.1 nm (FWHM) for the 15-mm-long grating. Further optimization of the refractive index profiles may result in $n_{eff,TE} = n_{eff,TM}$, i.e., polarization-independent filter properties, and the reflectivity should be enlarged to values close to 100% by increased substrate doping and/or additional annealing treatment.

4.2 Optical phase conjugation

Because of the high light intensities that can be achieved in waveguiding structures, optical phase conjugation in a planar waveguide may enable, in general, high efficiencies as well as a fast response time for the grating buildup. A drawback is the two-dimensional waveguide structure, which reduces the beam cleanup properties to only one dimension, because in the plane normal to the waveguiding plane the spatial intensity distribution of the light beam is restricted by the limited number of excitable modes. The use of waveguides with a large number of guided modes, i.e., a relatively thick waveguiding layer or, in other words, a thin bulk crystal, may avoid this problem, and a nearly two-dimensional phase conjugation becomes possible; however, in this case the intensity inside the sample is considerably reduced when compared to thin waveguides, which have a typical thickness of only a few μm. On the other hand, applications for even single-mode waveguide phase conjugators may be possible, for example, laser diodes with planar cavity, or devices that use optical bistability, which is often connected with phase conjugation in photorefractive crystals [208]. In this section, two examples of phase conjugation are discussed, namely anisotropic four-wave mixing in LiNbO$_3$:Ti:Fe waveguides, and self-pumped phase conjugation in a H$^+$-implanted BaTiO$_3$ waveguide.

In contrast to isotropic four-wave mixing, where either signal or phase-conjugated waves are amplified by the nonlocal contribution of refractive index changes, in the anisotropic case both waves can simultaneously gain intensity from the pump beams [209]. We have used anisotropic wave mixing in both LiNbO$_3$ [17] and LiTaO$_3$ [141] waveguides for the efficient generation of phase-conjugated waves. Here beam coupling leads to the amplification of extraordinarily polarized light; thus two counterpropagating, TM polarized pump waves and a copropagating TE polarized signal wave have been used. In Fig. 11 anisotropic four-wave mixing in a planar LiNbO$_3$:Ti:Fe waveguide is shown [210]. The waveguide contains about 18 modes at a wavelength of 514.5 nm. Because of the high damping of about 3 cm^{-1} in the waveguide the outcoupled powers of the signal and the phase-conjugate beam are rather small. Nevertheless, for input powers of about 0.7 mW and an interaction length of 4.6 mm we have obtained phase-conjugate reflectivities exceeding values of one [211].
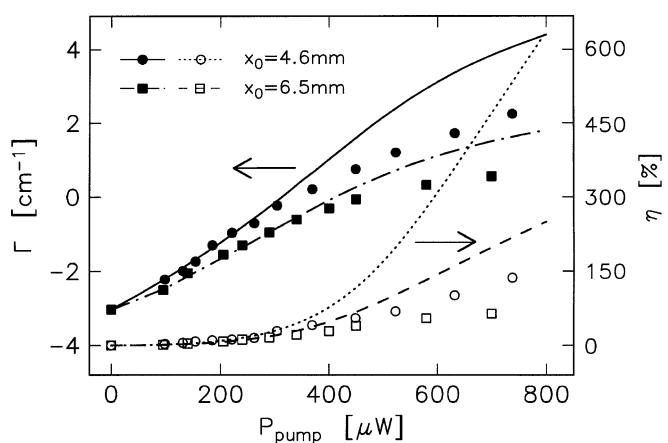
Fig. 11. Anisotropic four-wave mixing in a planar LiNbO$_3$:Ti:Fe waveguide [210]. Net signal wave gain Γ (*filled symbols*, experimental; *upper curves*, theoretical) and phase-conjugate reflectivity η (*open symbols*, experimental; *lower curves*, theoretical) as a function of input pump power P_{pump} for two different interaction lengths x_0
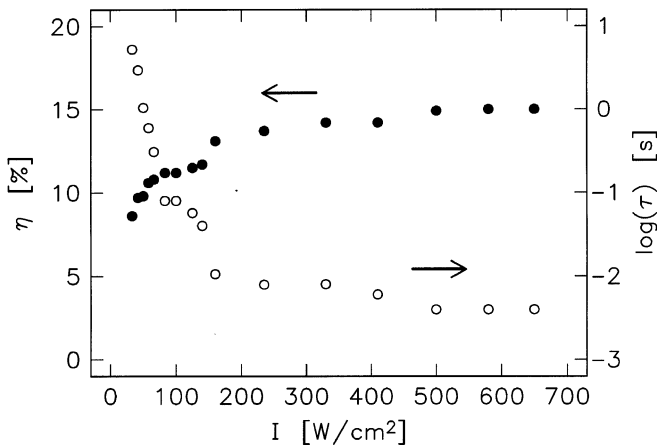
Fig. 12. Self-pumped phase conjugation in a H⁺-implanted BaTiO₃ wave-guide. Phase-conjugate efficiency η (●) and response time τ (○) are measured as a function of the input intensity (wavelength 488 nm) at the entrance face of the sample. Data are taken from [151]

Self-pumped phase conjugation in a planar waveguide was first reported by James et al. by using a H⁺-implanted BaTiO₃ crystal [151] (see Fig. 12). The multimode wave-guiding layer had a thickness of about 15 μm. Phase-conjugate reflectivities of 20% in the waveguide were achieved. The grating buildup time was reduced to some ms, a reduction by two orders of magnitude when compared with the same input power in the bulk. The fidelity of the sample for spatial cleanup of an input beam was limited by the finite number of modes, but in particular as well by the geometry of the sample, which resulted in an input-angle-dependent launch efficiency. Furthermore, in another experiment using the same BaTiO₃ sample, the operation of a bridge mutually pumped phase conjugator has been demonstrated [152].

4.3 Self-focusing and spatial solitons

For several years self-focusing and defocusing of light beams in photorefractive materials have been the subject of increasing interest, because these effects enable diffraction-free or soliton-like propagation of optical light waves [212–216]. Both bright and dark spatial solitons in photorefractive crystals have been investigated. A bright spatial soliton is a collimated light beam that propagates through the nonlinear material without changing its transverse profile. Diffraction is compensated by the self-focusing effect, i.e., by the light-induced positive refractive index changes in the plane perpendicular to the propagation direction of the optical beam. A dark soliton consists of a dark band, or notch, which is superimposed on an otherwise uniform background illumination. Here self-defocusing that is due to negative refractive index changes balances the diffraction of the notch.

In 1992/93 quasi-steady-state solitons that are transient in time evolution were predicted and studied in photorefractive crystals with an externally applied electric field [212, 213]. One year later, the existence of dark and bright steady-state photovoltaic solitons in materials subjected to the photovoltaic effect was demonstrated [214]. In the same year, in photorefractive crystals that were also biased with an external electric field, steady-state spatial solitons resulting

from a nonuniform screening of this external field were obtained [215, 216].

It has been experimentally confirmed that photorefractive spatial solitons may exist at optical powers of a few μW [217], which is some orders of magnitude lower than for Kerr-type solitons [218]. Among the most interesting properties of optical solitons is the nonlinear interaction that takes place when two solitons intersect or propagate close enough within the crystal [219]. In conjunction with the low power level these interacting forces between solitons promise potential applications as photonic elements, for example, all-optical switches, directional couplers, or beam deflectors [220, 221]. For some applications waveguide configurations are preferred, as they are compatible with semiconductor lasers and optical fiber technology, allow for the integration of other optical components (for example, phase shifters), and because of favorably modified photorefractive properties they may work at even lower power levels of the input light. In the following paragraphs, self-trapping of light beams in planar waveguides and their use for optical switching will be discussed.

4.3.1 Self-trapping of optical beams. For most of the recent experimental investigations of photorefractive spatial solitons in the bulk, strontium-barium niobate crystals have been used. In 1998 we showed that planar photorefractive waveguides can be used for the formation of spatial solitons, too [222]. Bright steady-state screening solitons have been realized in a He⁺-implanted SBN waveguide for visible and near-infrared light (wavelengths 514.5 to 780 nm). In the same waveguide, we have found transient self-focusing or quasi-steady-state solitons.

The formation of steady-state solitons for red light, starting from the initially divergent helium-neon laser beam (wavelength 632.8 nm), is illustrated in Fig. 13a as a function of the biasing electric field. For fields larger than 5 kV/cm a threshold behavior of the beam diameter is observed, and the light is trapped in the self-induced narrow waveguide channel with diameters of about 9 μm (see Fig. 13b). As in bulk crystals [223], the self-trapping of the beam is accompanied by a strong bending of the soliton's path because of the nonlocal contributions to the refractive index change by the photorefractive effect.

4.3.2 All-optical switching and routing. Different types of optical switches and interconnections using photorefractive waveguides have been experimentally investigated. Holographic interconnections in a planar LiNbO₃ waveguide have been proposed by Jannson [224] and further developed and experimentally confirmed by Brady and Psaltis [225]. The reconfigurable interconnections of different sets of input and output channel waveguides via thick holograms that are written by external unguided beams allow for large-scale linear transformations, for example, optical vector-matrix multipliers. A modified device may also be used for wavelength multiplexing. Aronson and Hesselink [226] have reported on an array of two sets of parallel channel waveguides in LiNbO₃ intersecting at right angles. In the iron-doped intersections dynamic holographic gratings were formed by the guided beams. Arrays of 50 × 50 waveguides were fabricated in an area of 25 cm², but the devices suffer from slow writing times of about 1 s. Itoh et al. have fabricated arrays of photorefractive waveguides for optically modifiable interconnections in
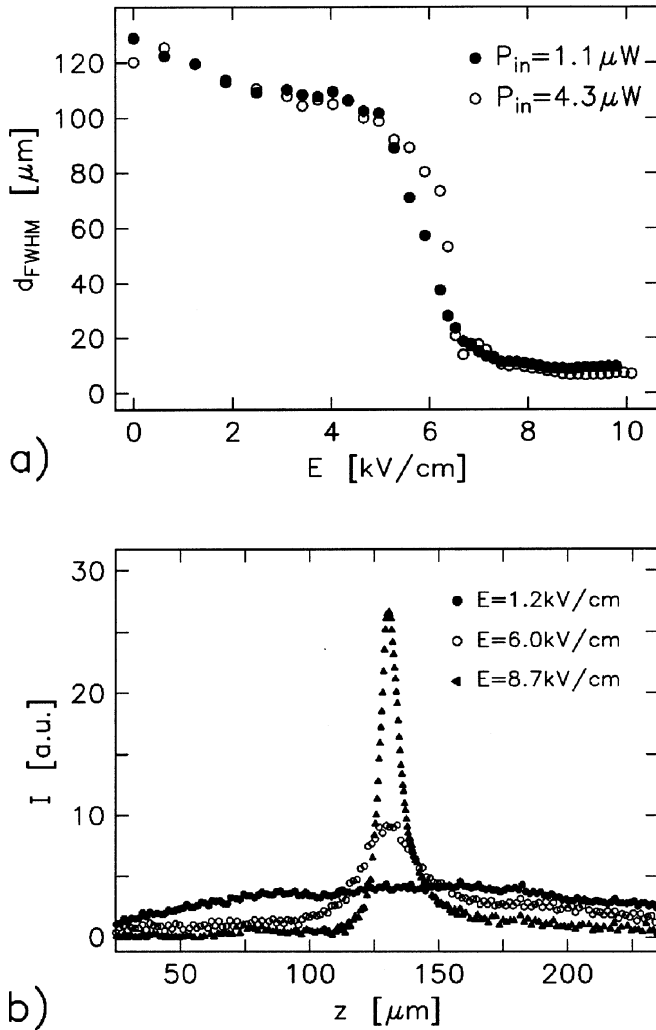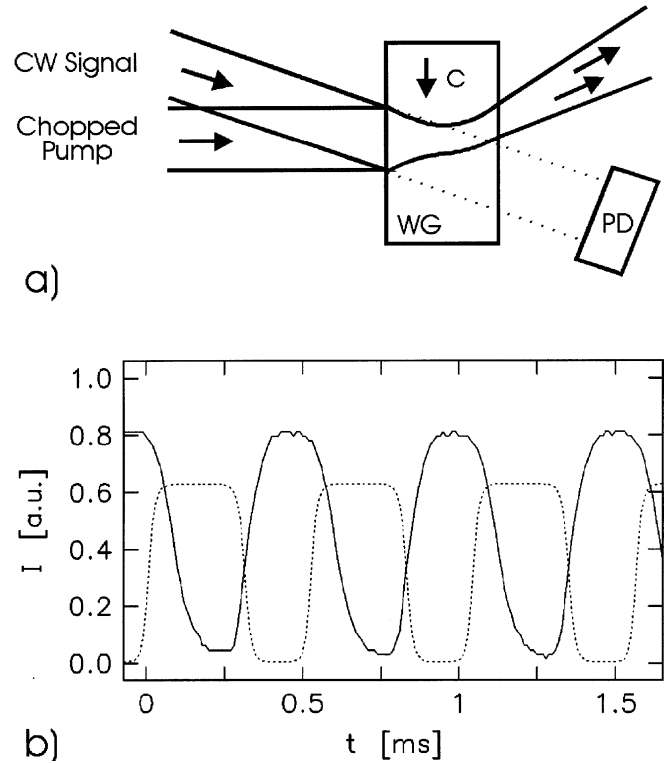
Fig. 13a,b. Steady-state spatial soliton formation in a biased He^+-implanted SBN waveguide [222]. **a** Beam diameter d (FWHM) at the exit face as a function of the externally applied electric field E and for two different input powers P_{in} of helium-neon laser light. **b** Intensity profiles $I(z)$ for the case $P_{in} = 4.3\,\mu W$ and different values of E . The background illumination of the whole sample with green light (wavelength 514.5 nm) is about $30\,mW/cm^2$

Fig. 14a,b. All-optical switching in a planar SBN waveguide [233]. **a** Interaction scheme of chopped pump (wavelength 514.5 nm) and cw signal beam (wavelength 632.8 nm) inside the waveguide (WG). The pump beam is self-focused and self-bent to the top, trapping the signal beam that moves away from the photodiode (PD). **b** Switching characteristic of the signal beam (*solid line*) for a frequency of 1.9 kHz of the mechanical chopper in the beam line of the pulsed pump beam (*dotted line*)

optical neural networks by illuminating a LiNbO$_3$ bulk crystal with an interference fringe pattern [227], or by scanning of an external focused laser beam [228, 229].

The formation of dynamic lenses in planar LiNbO$_3$ waveguides additionally doped with iron has recently been demonstrated by Shandarov [230]. The nonlinear lens formation is due to charge redistribution because of the photovoltaic effect and has time constants in the range of a few seconds to minutes. In the final stage, the photovoltaic lens leads to a defocusing of the input beam. The application of this self-lensing effect for all-optical switching has been proposed [231].

Another waveguide device that can be used for all-optical switching and beam deflection is based on a combination of the thermo-optic effect and photorefractive self-bending by the diffusion mechanism. Absorption of a guided light beam increases the temperature inside the waveguiding layer and yields a positive change of the refractive index because of the thermo-optic effect and the screening of the pyroelectric field. A strong self-induced focusing lens builds up within fractions

of ms [232]. In our switching experiment [233] that is illustrated in Fig. 14a, both a strongly absorbed green pump beam and a weakly absorbed red signal beam intersect inside the planar SBN waveguide. When the pump beam is switched on, a positive lens is formed that focuses the pump beam, and the signal beam is trapped in the induced channel with an increased refractive index, thus changing its original direction. Now the pump beam is self-focused to small diameters of a few μm, and another mechanism becomes effective: the beam is also self-bent in the direction of the negative c axis of the crystal because of diffusion of excited charge carriers. The already trapped signal beam which shows only little photorefractive effects follows the bent channel and moves away from the photodetector. Large deflection angles up to 0.23 rad have been obtained [233]. The switching behavior of the signal beam is given in Fig. 14b for a chopper frequency of 1.9 kHz, and similar results have been obtained for frequencies up to 3 kHz. By further improvement of the device much faster switching should be easily obtainable.

5 Conclusion

Recent results on formation and investigation of photorefractive waveguides have been summarized, and some interesting applications of these samples have been outlined. Further improvement and simplification of the necessary fabrication technologies, for example, by low-cost thin film deposition,

as well as tailored photorefractive properties and geometries of the waveguides will stimulate future developments of non-linear optical devices that are based on photorefractive effects.

References

1. A. Ashkin, G.D. Boyd, J.M. Dziedzic, R.G. Smith, A.A. Ballman, J.J. Levinstein, K. Nassau: Appl. Phys. Lett. **9**, 72 (1966)
2. P. Günter, J.-P. Huignard (Eds.): Photorefractive Materials and Their Applications I+II, Topics Appl. Phys., Vol. 61 and 62 (Springer, Berlin, Heidelberg 1988)
3. M.P. Petrov, S.I. Stepanov, A.V. Khomenko (Eds.): *Photorefractive Crystals in Coherent Optical Systems* (Springer, Berlin, Heidelberg 1991)
4. W. Karthe, R. Müller: *Integrierte Optik* (Akademische Verlagsgesellschaft, Leipzig 1991)
5. A.M. Prokhorov, Y.S. Kuzminov: *Ferroelectric Thin-Film Waveguides in Integrated Optics* (Cambridge International Science, Cambridge 1996)
6. V.E. Wood, P.J. Cressman, R.L. Holman, C.M. Verber: In Photorefractive Materials and Their Applications II, ed. by P. Günter, J.-P. Huignard, Topics Appl. Phys. Vol. 62 (Springer, Berlin, Heidelberg 1988)
7. R.V. Schmidt, I.P. Kaminow: Appl. Phys. Lett. **25**, 458 (1974)
8. R.J. Holmes, D.M. Smyth: J. Appl. Phys. **55**, 3531 (1984)
9. M. De Sario, M.N. Armenise, C. Canali, A. Carnera, P. Mazzoldi, G. Celotti: J. Appl. Phys. **57**, 1482 (1985)
10. S. Fries, P. Hertel, H.P. Menzler: Phys. Status Solidi A **108**, 449 (1988)
11. V.V. Atuchin, K.K. Ziling, D.P. Shipilova: Sov. J. Quantum Electron. **14**, 671 (1984)
12. A.D. Novikov, S.G. Odoulov, V.M. Shandarov, S.M. Shandarov: Sov. Phys. Tech. Phys. **33**, 969 (1988)
13. D. Kip, B. Gather, H. Bendig, E. Krätzig: Phys. Status Solidi A **139**, 241 (1993)
14. V.L. Popov, V.M. Shandarov: Sov. Phys. Tech. Phys. **36**, 1380 (1991)
15. V.M. Shandarov, S.M. Shandarov: Sov. Tech. Phys. Lett. **12**, 20 (1986)
16. A.I. Bashkirov, V.M. Shandarov: Sov. Phys. Tech. Phys. **34**, 882 (1989)
17. D. Kip, E. Krätzig: Opt. Lett. **17**, 1563 (1992)
18. W.M. Young, R.S. Feigelson, M.M. Fejer, M.F.J. Digonnet, H.J. Shaw: Opt. Lett. **16**, 995 (1991)
19. J.M. Hammer, W. Phillips: Appl. Phys. Lett. **24**, 545 (1974)
20. I.P. Kaminow, J.R. Carruthers: Appl. Phys. Lett. **22**, 326 (1973)
21. R.L. Holman, P.J. Cressman, J.F. Revelli: Appl. Phys. Lett. **32**, 280 (1978)
22. J.L. Jackel: J. Opt. Commun. **3**, 82 (1982)
23. A. Rasch, M. Rottschalk, W. Karthe: J. Opt. Commun. **6**, 14 (1985)
24. J.L. Jackel, C.E. Rice, J.J. Veselka: Ferroelectr. **50**, 165 (1983)
25. V.A. Ganshin, Y.N. Korkishko, T.V. Morozova, V.V. Saraikin: Phys. Status Solidi A **114**, 457 (1989)
26. K. Yamamoto, T. Taniuchi: J. Appl. Phys. **70**, 6663 (1991)
27. E.Y.B. Pun, K.K. Loi, P.S. Chung: IEEE Trans. Lightwave Technol. **11**, 277 (1993)
28. J.T. Cargo, A.J. Filo, M.C. Hughes, V.C. Kannan, F.A. Stevie, J.A. Taylor, J.R. Holmes: J. Appl. Phys. **67**, 627 (1990)
29. J.L. Jackel: Proc. SPIE **1583**, 54 (1991)
30. J.M. Cabrera, J. Olivares, M. Carrascosa, J. Rams, R. Müller, E. Dieguez: Adv. Phys. **45**, 349 (1996)
31. V.V. Atuchin, T.I. Zakharyash: Sov. Phys. Tech. Phys. **29**, 584 (1984)
32. K. Tada, T. Murai, T. Nakabayashi, T. Iwashima, T. Ishikawa: Jpn. J. Appl. Phys. **26**, 503 (1987)
33. V.A. Ganshin, V.S. Ivanov, Y.N. Korkishko, V.Z. Petrova: Sov. Phys. Tech. Phys. **31**, 794 (1986)
34. F. Rickermann, D. Kip, B. Gather, E. Krätzig: Phys. Status Solidi A **150**, 763 (1995)
35. Y.N. Korkishko, V.A. Fedorov: J. Appl. Phys. **82**, 1010 (1997)
36. R.A. Becker: Appl. Phys. Lett. **43**, 131 (1986)
37. M. Minakata, K. Kumagi, S. Kawakami: Appl. Phys. Lett. **49**, 992 (1986)
38. M. Rottschalk, A. Rasch, W. Karthe: J. Opt. Commun. **9**, 19 (1988)
39. I. Savatinova, S. Tochev, R. Todorov, M.N. Armenise, V.M.N. Passaro, C.C. Ziling: J. Lightwave Technol. **14**, 403 (1996)
40. P.G. Suchoski, T.K. Findakly, F.J. Leonberger: Opt. Lett. **13**, 1050 (1988)
41. N. Goto, G.L. Yip: Appl. Opt. **28**, 60 (1989)
42. S.M. Kostritskii, D. Kip, E. Krätzig: Appl. Phys. B **65**, 517 (1997)
43. S.M. Kostritskii, O.M. Kolesnikov: J. Opt. Soc. Am. B **11**, 1674 (1994)
44. Y.A. Bobrov, V.A. Ganshin, V.S. Ivanov, Y.N. Korkishko, T.V. Morozova: Phys. Status Solidi A **123**, 317 (1991)
45. V.A. Ganshin, Y.N. Korkishko: Sov. Phys. Tech. Phys. **29**, 227 (1984)
46. G.L. Destefanis, J.P. Gailliard, E.L. Ligeon, S. Valette, B.W. Farmery, P.D. Townsend, A. Perez: J. Appl. Phys. **50**, 7898 (1979)
47. P. Moretti, P. Thevenard, G. Godefroy, R. Sommerfeld, P. Hertel, E. Krätzig: Phys. Status Solidi A **117**, K85 (1990)
48. T. Bremer, W. Heiland, B. Hellermann, P. Hertel, E. Krätzig, D. Kollewe: Ferroelectr. Lett. **9**, 11 (1988)
49. P. Moretti, P. Thevenard, K. Wirl, P. Hertel, H. Hesse, E. Krätzig, G. Godefroy: Ferroelectr. **128**, 13 (1992)
50. D. Kip, S. Mendricks, P. Moretti: Phys. Status Solidi A **166**, R3 (1998)
51. D. Kip, S. Aulkemeyer, P. Moretti: Opt. Lett. **20**, 1256 (1995)
52. J.F. Ziegler, J.P. Biersack (Eds.): *Stopping and Ranges of Ions in Matter* (Pergamon, New York, 1985)
53. J.Y.C. Wong, L. Zhang, G. Kakarantzas, P.D. Townsend, P.J. Chandler, L.A. Boatner: J. Appl. Phys. **71**, 49 (1992)
54. T. Pliska, D. Fluck, P. Günter, L. Beckers, C. Buchal: J. Opt. Soc. Am. B **15**, 628 (1998)
55. L. Zhang, P.J. Chandler, P.D. Townsend: Nucl. Instrum. Methods B **59/60**, 1147 (1991)
56. D. Fluck, D.H. Jundt, P. Günter, M. Fleuster, C. Buchal: J. Appl. Phys. **74**, 6023 (1993)
57. P.D. Townsend: Nucl. Instrum. Methods B **46**, 18 (1990)
58. F.P. Strohkendl, D. Fluck, P. Günter, R. Irmscher, C. Buchal: Appl. Phys. Lett. **59**, 3354 (1991)
59. D. Fluck, P. Günter, M. Fleuster, C. Buchal: J. Appl. Phys. **72**, 1671 (1992)
60. K.K. Schuegraf (Ed.): *Handbook of Thin Film Deposition: Processes and Techniques* (Noyes Publications, New Jersey 1988)
61. D.A. Glocker, S.I. Shah (Eds.): *Handbook of Thin Film Process Technology* (IOP Publishing, Bristol 1995)
62. W.S. Hu, Z.G. Liu, Y.-Q. Lu, S.N. Zhu, D. Feng: Opt. Lett. **21**, 946 (1996)
63. A. Ito, A. Machida, M. Obara: Jpn. J. Appl. Phys. **36**, L805 (1997)
64. C. Zaldo, D.S. Gill, R.W. Eason, J. Mendiola, P.J. Chandler: Appl. Phys. Lett. **65**, 502 (1994)
65. D. Trivedi, P. Tayebati, M. Tabat: Appl. Phys. Lett. **68**, 3227 (1996)
66. F. Gitmans, Z. Sitar, P. Günter: Vacuum **46**, 939 (1995)
67. R.A. McKee, F.J. Walker, J.R. Conner, E.D. Specht, D.E. Zelmon: Appl. Phys. Lett. **59**, 782 (1991)
68. A. Baudrant, H. Vial, J. Daval: J. Cryst. Growth **43**, 197 (1978)
69. R.R. Neurgaonkar, E.T. Wu: Mater. Res. Bull. **22**, 1095 (1987)
70. B. Bihari, J. Kumar, G.T. Stauf, P.C. Van Bushirk, C.S. Hwang: J. Appl. Phys. **76**, 1169 (1994)
71. H. Xie, W.-H. Hsu, R. Raj: J. Appl. Phys. **77**, 3420 (1995)
72. M.J. Nystrom, B.W. Wessels, W.P. Lin, G.K. Wong, D.A. Neumayer, T.J. Marks: Appl. Phys. Lett. **66**, 1726 (1995)
73. T. Hayashi, N. Ohji, K. Hirohara, T. Fukunaga, H. Maiwa: Jpn. J. Appl. Phys. **32**, 4092 (1993)
74. Y. Xu, C.J. Chen, R. Xu, J.D. Mackenzie: Phys. Rev. B **44**, 35 (1991)
75. O. Eknoyan, H.F. Taylor, Z. Tang, V.P. Svenson, J.M. Marx: Appl. Phys. Lett. **60**, 407 (1992)
76. P.K. Tien, R. Ulrich: J. Opt. Soc. Am. **60**, 1325 (1970)
77. J.M. White, P.F. Heidrich: Appl. Opt. **15**, 151 (1976)
78. K.S. Chiang: J. Lightwave Technol. **3**, 385 (1985)
79. P. Hertel, H.P. Menzler: Appl. Phys. B **44**, 75 (1987)
80. S. Herminghaus, B.A. Smith, J.D. Swalen: J. Opt. Soc. Am. B **8**, 2311 (1991)
81. T. Yuhara, K. Tada, Y.-S. Li: J. Appl. Phys. **71**, 3966 (1992)
82. P. Tayebati, D. Trivedi, M. Tabat: Appl. Phys. Lett. **69**, 1023 (1996)
83. T. Suzuki, O. Eknoyan, H.F. Taylor: J. Lightwave Technol. **11**, 285 (1993)
84. R.A. Rupp: Appl. Phys. A **55**, 2 (1992)
85. V.E. Wood, N.F. Hartman, C.M. Verber, R.P. Kenan: J. Appl. Phys. **46**,

1214 (1975)

86. D. Kip, R. Fink, T. Bartholomäus, E. Krätzig: Opt. Commun. **95**, 33 (1993)

87. W. Yu, W. Krolikowski, B. Luther-Davis, M. Webster, M. Asutin: Opt. Lett. **20**, 563 (1995)

88. J. Hukriede, D. Kip, E. Krätzig: Appl. Phys. Lett. **66**, 333 (1998)

89. N.V. Kukhtarev, V.B. Markov, S.G. Odoulov, M.S. Soskin, V.L. Vinetskii: Ferroelectr. **22**, 949 (1979)

90. H. Kogelnik: Bell Syst. Tech. J. **48**, 2909 (1969)

91. V. Gericke, P. Hertel, E. Krätzig, J.P. Nisius, R. Sommerfeld: Appl. Phys. B **44**, 155 (1987)

92. D. Fluck, J.A. Weiss, S. Brülisauer, P. Günter: Opt. Lett. **19**, 2080 (1994)

93. M. Aguilar, M. Carrascosa, F. Agullo-Lopez, L.F. Magana: J. Appl. Phys. **78**, 4840 (1995)

94. D. Kip, F. Rickermann, E. Krätzig: Opt. Lett. **20**, 1139 (1995)

95. L. Wan, Y. Yuan, G. Assanto: Opt. Commun. **73**, 439 (1989)

96. L. Wan, Y. Yuan, G. Assanto: Opt. Commun. **74**, 361 (1990)

97. A. Yamada, H. Tamada, M. Saitoh: J. Appl. Phys. **76**, 1776 (1994)

98. K. Buse: Appl. Phys. B **64**, 391 (1997)

99. R.V. Schmidt, I.P. Kaminow: IEEE J. Quantum Electron. **QE-11**, 57 (1975)

100. R. Göring, Z. Yuan-Ling, S. Steinberg: Appl. Phys. A **55**, 97 (1992)

101. K. Buse: Appl. Phys. B **64**, 273 (1997)

102. F. Jermann, J. Otten: J. Opt. Soc. Am. B **10**, 2085 (1993)

103. Y. Kondo, S. Miyaguchi, A. Onoe, Y. Fujii: Appl. Opt. **33**, 3348 (1994)

104. J. Jackel, A.M. Glass, G.E. Petersen, C.E. Rice, D.H. Olsen, J.J. Veleska: J. Appl. Phys. **55**, 269 (1984)

105. J. Olivares, E. Dieguez, F.J. Lopez, J.M. Cabrera: Appl. Phys. Lett. **61**, 624 (1992)

106. A. Yamada, H. Tamada, M. Saitoh: J. Cryst. Growth **132**, 48 (1993)

107. Y. Kondo, T. Kouyama, K. Ohno, M. Tsuji, M. Nakamura, Y. Fujii: Jpn. J. Appl. Phys. **33**, L338 (1994)

108. S. Schwyn, H.W. Lehmann, R. Widmer: J. Appl. Phys. **72**, 1154 (1991)

109. S. Tan, T. Gilbert, C.-Y. Hung, T.E. Schlesinger, M. Migliuolo: J. Appl. Phys. **79**, 3548 (1996)

110. K. Nashimoto, M.J. Cima: Mater. Lett. **10**, 348 (1991)

111. J.-M. Liu, Z.G. Liu, S.N. Zhu, Z.C. Wu: Mater. Lett. **20**, 35 (1994)

112. I.I. Itkin, S.M. Shandarov: Sov. Phys. Tech. Phys. **35**, 1317 (1990)

113. P.G. Kazansky: IEEE J. Quantum Electron. **QE-25**, 736 (1989)

114. E.S. Shandarov, S.M. Shandarov: Opt. and Spectrosc. **69**, 824 (1990)

115. A.D. Novikov, S.G. Odoulov, V.M. Shandarov, E.S. Shandarov, S.M. Shandarov: J. Opt. Soc. Am. B **8**, 1298 (1991)

116. V.L. Popov, E.S. Shandarov, S.M. Shandarov: J. Opt. Soc. Am. B **9**, 1661 (1992)

117. G. Glazov, V.M. Shandarov, E.S. Shandarov, S.M. Shandarov: J. Opt. Soc. Am. B **7**, 2279 (1990)

118. G. Glazov, E.S. Shandarov, S.M. Shandarov: Int. J. Nonl. Opt. Phys. **2**, 71 (1993)

119. E.M. Zolotov, P.G. Kazansky, V.A. Chernykh: Sov. Tech. Phys. Lett. **7**, 397 (1981)

120. I.I. Itkin, S.M. Shandarov: Sov. Tech. Phys. Lett. **16**, 357 (1990)

121. V.I. Belinicher, B.I. Sturman: Sov. Phys.: Uspheki **23**, 199 (1980)

122. S.G. Odoulov: Sov. Phys. JETP Lett. **35**, 10 (1982)

123. I.I. Itkin, S.M. Shandarov: Avtometriya **4**, 72 (1989)

124. Y. Solomonov, S.M. Shandarov, V.M. Shandarov: Ferroelectr. **201**, 195 (1997)

125. D. Kip, E. Krätzig: Proc. of the International Conference on Lasers 1992 (Lasers '92), Houston (USA), 1992, p. 499

126. U.B. Ramabadran, H.E. Jackson, J.T. Boyd: J. Appl. Phys. **74**, 1492 (1993)

127. T. Fujiwara, S. Sato, H. Mori: Appl. Phys. Lett. **54**, 975 (1989)

128. T. Fujiwara, X. Cao, R. Srivastava, R.V. Ramaswamy: Appl. Phys. Lett. **61**, 743 (1992)

129. T. Fujiwara, R. Srivastava, X. Cao, R.V. Ramaswamy: Opt. Lett. **18**, 346 (1993)

130. S. Steinberg, R. Göring, T. Hennig, A. Rasch: Opt. Lett. **20**, 683 (1995)

131. M. Rottschalk, T. Bachmann, S. Steinberg, J.-P. Ruske: Opt. Commun. **106**, 187 (1994)

132. E.E. Robertson, R.W. Eason, Y. Yokoo, P.J. Chandler: Appl. Phys. Lett. **70**, 2094 (1997)

133. D. Eger, M.A. Arbore, M.M. Fejer, M.L. Bortz: J. Appl. Phys. **82**, 998 (1997)

134. H. Yoshinaga, K. Kitayama, H. Oguri: Appl. Phys. Lett. **56**, 1728 (1990)

135. F. Ito, K. Kitayama, H. Oguri: J. Opt. Soc. Am. B **9**, 1432 (1992)

136. S. Yin: Proc. SPIE **2849**, 156 (1996)

137. W.B. Spillman, N.A. Sanford, R.A. Soref: Opt. Lett. **8**, 497 (1983)

138. V.A. Fedorov, V.A. Ganshin, Y.N. Korkishko, T.V. Morozova: Ferroelectr. **138**, 23 (1993)

139. O. Eknoyan, H.F. Taylor, W. Matous, T. Ottinger, R.R. Neurgaonkar: Appl. Phys. Lett. **71**, 3051 (1997)

140. Y. Kondo, Y. Fujii: Jpn. J. Appl. Phys. **34**, L365 (1995)

141. D. Kip, T. Bartholomäus, P.M. Garcia, E. Krätzig: J. Opt. Soc. Am. B **11**, 1737 (1994)

142. S. Kostritskii, D. Kip, E. Krätzig: Technical Digest of the Topical Meeting on "Photorefractive Materials, Effects, and Devices 1997" (PRM '97), Chiba, Japan, 1997, p. 216

143. S. Kostritskii, D. Kip: Holographic recording in planar Cu:H:LiTaO$_3$ waveguides, sent to Phys. Status Solidi A

144. L.S. Hung, J.A. Agostinelli, J.M. Mir, L.R. Zheng: Appl. Phys. Lett. **62**, 3071 (1993)

145. J.A. Agostinelli, G.H. Braustein, T.N. Blanton: Appl. Phys. Lett. **63**, 123 (1993)

146. X.L. Guo, Z.G. Liu, S.N. Zhu, T. Yu, S.B. Xiong, W.S. Hu: J. Cryst. Growth **165**, 187 (1996)

147. T. Tschudi, A. Herden, J. Goltz, H. Klumb, F. Laeri, J. Albers: IEEE J. Quantum Electron. **QE-22**, 1493 (1986)

148. Z. Zhang, Y. Zhang, C. Yang, J. Kang, S. Zheng, Y. Zhu, Y. Chen, X. Wu, P. Fu: J. Opt. Soc. Am. B **11**, 1991 (1994)

149. P. Moretti, P. Thevenard, R. Sommerfeld, G. Godefroy: Nucl. Instrum. Methods B **59/60**, 1228 (1991)

150. K.E. Youden, S.W. James, R.W. Eason, P.J. Chandler, L. Zhang, P.D. Townsend: Opt. Lett. **17**, 1509 (1992)

151. S.W. James, K.E. Youden, P.M. Jeffrey, R.W. Eason, P.J. Chandler, L. Zhang, P.D. Townsend: Opt. Lett. **18**, 1138 (1993)

152. S.W. James, K.E. Youden, P.M. Jeffrey, R.W. Eason, P.J. Chandler, L. Zhang, P.D. Townsend: Appl. Opt. **32**, 5299 (1993)

153. F. Ito, K. Kitayama, K. Tomomatsu: Appl. Phys. Lett. **61**, 2144 (1992)

154. D. Roy, S.B. Krupanidhi: Appl. Phys. Lett. **61**, 2057 (1992)

155. D.M. Gill, B.A. Block, C.W. Conrad, B.W. Wessels, S.T. Ho: Appl. Phys. Lett. **69**, 2968 (1996)

156. D.M. Gill, C.W. Conrad, G. Ford, B.W. Wessels, S.T. Ho: Appl. Phys. Lett. **71**, 1783 (1997)

157. Y. Liu, Z. Chen, C. Li, D. Cui, Y. Zhou, G. Yang: J. Appl. Phys. **81**, 6328 (1997)

158. L. Beckers, J. Schubert, W. Zander, J. Ziesmann, A. Eckau, P. Leinenbach, C. Buchal: J. Appl. Phys. **83**, 3305 (1998)

159. P. Günter: Phys. Rep. **93**, 199 (1982)

160. F.P. Strohkendl, P. Günter, C. Buchal, R. Irmscher: J. Appl. Phys. **69**, 84 (1991)

161. S. Brülisauer, D. Fluck, P. Günter: Electron. Lett. **31**, 312 (1995)

162. S. Brülisauer, D. Fluck, P. Günter, L. Beckers, C. Buchal: J. Opt. Soc. Am. B **13**, 2544 (1996)

163. D. Fluck, P. Günter, R. Irmscher, C. Buchal: Appl. Phys. **59**, 3213 (1991)

164. M. Zha, D. Fluck, P. Günter, M. Fleuster, C. Buchal: Opt. Lett. **18**, 577 (1993)

165. R. Gutmann, J. Hulliger: Cryst. Prop. Prep. **32–34**, 117 (1991)

166. T.M. Graettinger, S.H. Rou, M.S. Ameen, O. Auciello, A.I. Kingon: Appl. Phys. Lett. **58**, 1964 (1991)

167. S. Schwyn, H.W. Lehmann, P. Günter: Appl. Phys. Lett. **61**, 373 (1992)

168. M.J. Martin, J.E. Alfonso, J. Mendiola, C. Zaldo, D.S. Gill, R.W. Eason, P.J. Chandler: J. Mater. Res. **12**, 2699 (1997)

169. M.D. Ewbank, R.R. Neurgaonkar, W.K. Cory, J. Feinberg: J. Appl. Phys. **62**, 374 (1987)

170. J. Ma, T. Chang, J. Hong, R.R. Neurgaonkar, G. Barbastathis, D. Psaltis: Opt. Lett. **22**, 1116 (1997)

171. G.L. Wood, W.W. Clark III, M.J. Miller, E.J. Sharp, G.J. Salamo, R.R. Neurgaonkar: IEEE J. Quantum Electron. **QE-23**, 2126 (1987)

172. R.R. Neurgaonkar, W.F. Hall, J.R. Oliver, W.W. Ho, W.K. Cory: Ferroelectr. **87**, 167 (1988)

173. R.A. Vazquez, M.D. Ewbank, R.R. Neurgaonkar: Opt. Commun. **80**, 253 (1991)

174. O. Eknoyan, C.H. Bulmer, H.F. Taylor, W.K. Burns, A.S. Greenblatt, L.A. Beech, R.R. Neurgaonkar: Appl. Phys. Lett. **48**, 13 (1986)

150

175. O. Eknoyan, V.P. Svenson, J.D. Quinn, R.R. Neurgaonkar: Appl. Phys. Lett. **59**, 28 (1991)
176. E.E. Robertson, R.W. Eason, M. Kaczmarek, P.J. Chandler, X. Huang: Opt. Lett. **21**, 641 (1996)
177. D. Kip, B. Kemper, I. Nee, R. Pankrath, P. Moretti: Appl. Phys. B **65**, 511 (1997)
178. D. Kip, B. Kemper, K. Buse, P. Moretti, E. Krätzig: Technical Digest of the Topical Meeting on Photorefractive Materials, Effects, and Devices 1997 (PRM '97), Chiba, Japan, 1997, p. 442
179. K. Buse, U. van Stevendaal, R. Pankrath, E. Krätzig: J. Opt. Soc. Am. B **13**, 1461 (1996)
180. V.D. Antsigin, V.M. Egorov, E.G. Kostsov, V.K. Malinovsky, L.N. Sterelyukhina: Ferroelectr. **63**, 235 (1985)
181. Y.Y. Zhu, R.F. Xiao, G.K.L. Wong: J. Appl. Phys. **82**, 4908 (1997)
182. D. Kip, S. Aulkemeyer, K. Buse, F. Mersch, R. Pankrath, E. Krätzig: Phys. Status Solidi A **154**, K5 (1996)
183. L. Hesselink, S. Redfield: Opt. Lett. **13**, 877 (1988)
184. Y. Sugiyama, S. Yagi, I. Yokohama, I. Hatakeyama: Jpn. J. Appl. Phys. **31**, 708 (1992)
185. M. Miyagi, Y. Sugiyama, S. Yagi, I. Hatakeyama: Jpn. J. Appl. Phys. **33**, L1417 (1994)
186. J.M. Marx, Z. Tang, O. Eknoyan, H.F. Taylor, R.R. Neurgaonkar: Appl. Phys. Lett. **66**, 274 (1995)
187. J.M. Marx, O. Eknoyan, H.F. Taylor, R.R. Neurgaonkar: IEEE Photon. Tech. Lett. **8**, 1024 (1996)
188. E.I. Leonov, S.E. Khabarov, M.S. Vershinin, V.A. Gusev, V.M. Orlov, L.G. Khokha: Sov. Phys. Tech. Phys. **30**, 1307 (1985)
189. K.E. Youden, R.W. Eason, M.C. Gower, N.A. Vainos: Appl. Phys. Lett. **59**, 1929 (1991)
190. V. Chevrier, A. Inam, S. Etemad, D. Harris, J.C. Launay: Technical Digest of the Topical Meeting on Photorefractive Materials, Effects, and Devices 1993 (PRM '93), Kiev, Ukraine, 1993, p. 220
191. Y.F. Kargin, I.V. Tsiar, Y.R. Salikaev, S.M. Shandarov: Tech. Phys. Lett. **20**, 997 (1994)
192. Y. Salikaev, S.M. Shandarov, Y. Kargin: Proc. SPIE **2795**, 203 (1996)
193. V.V. Prokofiev, J.P. Andreeta, C.J. de Lima, M.R.B. Andreeta, A.C. Hernandes, J.F. Carvalho, A.A. Kamshilin, T. Jääskeläinen: J. Cryst. Growth **137**, 528 (1994)
194. D. Fluck, R. Gutmann, P. Günter, R. Irmscher: J. Appl. Phys. **70**, 5147 (1991)
195. F. Lu, M.Q. Meng, K.M. Wang, F.X. Wang, W. Li, L.Z. Cai, Y.R. Wang, H.C. Chen, D.Y. Shen: Opt. Commun. **140**, 204 (1997)
196. W. Krolikowski, M. Cronin-Golomb, B.S. Chen: Appl. Phys. Lett. **57**, 7 (1990)
197. X. Yue, S. Mendricks, Y. Hu, H. Hesse, D. Kip: J. Appl. Phys. **83**, 3473 (1998)
198. C.T.A. Brown, J. Amin, D.P. Shepherd, A.C. Tropper, M. Hempstead: Opt. Lett. **22**, 1778 (1997)
199. C. Becker, A. Greiner, T. Oesselke, A. Pape, W. Sohler, H. Suche: Technical Digest of the Conference on Integrated Photonic Research 1998 (IPR '98), Victoria, Canada (1998)
200. R. Müller, M.T. Santos, L. Arizmendi, J.M. Carbera: J. Phys. D: Appl. Phys. **27**, 241 (1994)
201. H. Nishihara: Proc. 7th Eur. Conf. on Int. Opt. (ECIO '95), Delft (Netherlands), 1995, p. 249
202. W. Liu, E. Strzelecki, T. Jannson: Proc. SPIE **1635**, 20 (1990)
203. V. Minier, A. Kevorkian, J.M. Xu: IEEE Photon. Tech. Lett. **4**, 1115 (1992)
204. Y. Qiao, S. Orlov, D. Psaltis, R.R. Neurgaonkar: Opt. Lett. **18**, 1004 (1993)
205. J.J. Amodei, D.L. Staebler: Appl. Phys. Lett. **18**, 540 (1971)
206. K. Buse, S. Breer, K. Peithmann, S. Kapphan, M. Gao, E. Krätzig: Phys. Rev. B **56**, 1225 (1997)
207. J. Hukriede, I. Nee, D. Kip, E. Krätzig: Opt. Lett. **23** (1998), in press
208. S.W. James, R.W. Eason: Opt. Lett. **16**, 551 (1991)
209. A.D. Novikov, S.G. Odoulov, O. Oleinik, B.I. Sturman: Ferroelectr. **75**, 295 (1987)
210. D. Kip, E. Krätzig: Radiat. Eff. Defect. Solids **136**, 123 (1995)
211. D. Kip, E. Krätzig: Technical Digest of the Topical Meeting on Photorefractive Materials, Effects, and Devices 1993 (PRM '93), Kiev, Ukraine, 1993, p. 318
212. M. Segev, B. Crosignani, A. Yariv, B. Fischer: Phys. Rev. Lett. **68**, 923 (1992)
213. G. Duree, J.L. Schultz, G. Salamo, M. Segev, A. Yariv, B. Crosignani, P. DiPorto, E. Sharp, R.R. Neurgaonkar: Phys. Rev. Lett. **71**, 533 (1993)
214. G.C. Valley, M. Segev, B. Crosignani, A. Yariv, M.M. Fejer, M.C. Bashaw: Phys. Rev. A **50**, R4457 (1994)
215. M.D. Iturbe-Castillo, P.A. Marquez-Aguilar, J.J. Sanchez-Mondragon, S. Stepanov, V. Vysloukh: Appl. Phys. Lett. **64**, 408 (1994)
216. M. Segev, G.C. Valley, B. Crosignani, P. DiPorto, A. Yariv: Phys. Rev. Lett. **73**, 3211 (1994)
217. M.F. Shih, M. Segev, G.C. Valley, G. Salamo, B. Crosignani, P. DiPorto: Electron. Lett. **31**, 826 (1995)
218. M. Shalaby, A.J. Barthelemy: IEEE J. Quantum Electron. **QE-28**, 2736 (1992)
219. W. Krolikowski, S.A. Holmstrom: Opt. Lett. **22**, 369 (1997)
220. E.D. Eugenieva, R.V. Roussev, S.G. Dinev: J. Mod. Opt. **44**, 1127 (1997)
221. A.W. Snyder, A.P. Sheppard: Opt. Lett. **18**, 482 (1993)
222. D. Kip, M. Wesner, V.M. Shandarov, P. Moretti: Opt. Lett. **23**, 921 (1998)
223. M.F. Shih, P. Leach, M. Segev, M.H. Garret, G. Salamo, G.C. Valley Opt. Lett. **21**, 324 (1996)
224. T. Jannson: J. Opt. Soc. Am. **71**, 342 (1981)
225. D.J. Brady, D. Psaltis: Appl. Opt. **30**, 2324 (1991)
226. L.B. Aronson, L. Hesselink: Opt. Lett. **15**, 30 (1990)
227. O. Matoba, K. Itoh, Y. Ichioka: Opt. Lett. **21**, 122 (1996)
228. K. Itoh, O. Matoba, Y. Ichioka: Opt. Lett. **19**, 652 (1994)
229. O. Matoba, K. Itoh, Y. Ichioka: Opt. Eng. **35**, 2175 (1996)
230. V.M. Shandarov: Ferroelectr. **201**, 185 (1997)
231. V.M. Shandarov, S.M. Shandarov: Proc. SPIE **2969**, 158 (1996)
232. D. Kip, E. Krätzig, V.M. Shandarov, P. Moretti: Opt. Lett. **23**, 343 (1998)
233. D. Kip, M. Wesner, E. Krätzig, V.M. Shandarov, P. Moretti: Appl. Phys. Lett. **72**, 1960 (1998)